

AN OVERVIEW OF THE ROTATIONAL BEHAVIOR OF METAL-POOR STARS

C. CORTÉS¹, J. R. P. SILVA², A. RECIO-BLANCO³, M. CATELAN^{4,5,6}, J. D. DO NASCIMENTO JR.¹, J. R. DE MEDEIROS¹

Printed 2009 September 24 in ApJ

ABSTRACT

The present paper describes the behavior of the rotational velocity in metal-poor stars ($[\text{Fe}/\text{H}] \leq -0.5$ dex) in different evolutionary stages, based on $v \sin i$ values from the literature. Our sample is comprised of stars in the field and some Galactic globular clusters, including stars on the main sequence, the red giant branch (RGB), and the horizontal branch (HB). The metal-poor stars are, mainly, slow rotators, and their $v \sin i$ distribution along the HR diagram is quite homogeneous. Nevertheless, a few moderate to high values of $v \sin i$ are found in stars located on the main sequence and on the HB. We show that the overall distribution of $v \sin i$ values is basically independent of metallicity for the stars in our sample. In particular, the fast-rotating main sequence stars in our sample present similar rotation rates as their metal-rich counterparts, suggesting that some of them may actually be fairly young, in spite of their low metallicity, or else that at least some of them would be better classified as blue straggler stars. We do not find significant evidence of evolution in $v \sin i$ values as a function of position on the RGB; in particular, we do not confirm previous suggestions that stars close to the RGB tip rotate faster than their less evolved counterparts. While the presence of fast rotators among moderately cool blue HB stars has been suggested to be due to angular momentum transport from a stellar core that has retained significant angular momentum during its prior evolution, we find that any such transport mechanisms must likely operate very fast as the star arrives on the zero-age HB (ZAHB), since we do not find a link between evolution off the ZAHB and $v \sin i$ values.

We present an extensive tabulation of all quantities discussed in this paper, including rotation velocities, temperatures, gravities, and metallicities $[\text{Fe}/\text{H}]$, as well as broadband magnitudes and colors.

Subject headings: Stars: evolution – Stars: fundamental parameters – Stars: Population II – Stars: rotation – Stars: statistics

1. INTRODUCTION

Rotation has long been an important factor affecting stellar evolution that has been largely ignored, especially when dealing with unresolved stellar populations, since the interplay between rotation and evolution is very difficult to accurately establish. Still, knowledge of stellar angular momentum evolution and its influence on a star's evolutionary history is clearly crucial to properly understand the evolution of stars. In spite of its importance in stellar astrophysics, the influence of rotation upon stellar evolution has not been properly established yet, and there have been relatively few studies dedicated to this subject. Recently, the new space telescopes dedicated to asteroseismology and the search for extra-solar planets, such as CoRoT and Kepler, have opened the possibility to determine rotation periods for large samples of stars in the solar neighborhood covering all main evolutionary stages. These observations, and the information that we can derive therefrom, can give us keys for the study of the angular momentum evolution and their effects on the stellar life – and, as a main result, the Sun's evolution.

On the other hand, during the last two decades several studies have been aimed at describing rotation in metal-poor stars

(e.g., Peterson 1983; Peterson 1985a,b; Peterson et al. 1995; Cohen & McCarthy 1997; Behr et al. 2000a,b; Kinman et al. 2000; Behr 2003a,b; Carney et al. 2003, Recio-Blanco et al. 2002, 2004; De Medeiros et al. 2006; Carney et al. 2008). While these studies have led to a large list of high-precision $v \sin i$ measurements for metal-poor stars, a comprehensive study of the rotational behavior of metal-poor stars based on these data has not been performed yet. Since metal-poor stars are mainly members of the oldest stellar populations, such a dataset may help shed light on the evolution of the angular momentum over a large range of evolutionary stages for low-mass stars.

The distributions of $v \sin i$ in different evolutionary stages, from the main sequence (MS) to the red giant branch (RGB), as derived in these previous studies, show that metal-poor stars present, essentially, low $v \sin i$ values. Nevertheless, the stars in the horizontal branch (HB) do not show the same behavior and an enhanced rotation in these core helium-burning stars has been reported in several Galactic globular clusters (GCs) (e.g., Peterson et al. 1995; Cohen & McCarthy 1997; Behr et al. 2000a,b; Recio-Blanco et al. 2002, 2004). The stars in these dense environments present a broad range of $v \sin i$ values, from several km s^{-1} to tens of km s^{-1} . This particular distribution is not explained as a natural evolution of the stellar angular momentum, since their ancestors, the RGB stars, present lower $v \sin i$ values. Field HB stars seem to have a similar distribution of $v \sin i$ values (Kinman et al. 2000; Behr 2003b; Carney et al. 2003), suggesting that the environment does not play a strong role in defining the observed spread in $v \sin i$. Peterson et al. (1996) reported that the RR Lyrae stars, the variable stars located on the HB, present

¹ Departamento de Física, Universidade Federal do Rio Grande do Norte, 59072-970 Natal, RN, Brazil.

² Departamento de Física, Universidade do Estado do Rio Grande do Norte, Mossoró, RN., Brazil.

³ Observatoire de la Côte d'Azur, Nice, France.

⁴ Departamento de Astronomía y Astrofísica, Pontificia Universidad Católica de Chile, Santiago, Chile.

⁵ John Simon Guggenheim Memorial Foundation Fellow

⁶ On sabbatical leave at Departamento de Física, Universidade Federal do Rio Grande do Norte, 59072-970 Natal, RN, Brazil

an upper limit of $v \sin i \sim 10 \text{ km s}^{-1}$, indicating that these stars are also slow rotators and do not show the spread in $v \sin i$ found among other HB stars.

Soker (1998) and Soker & Harpaz (2000) have suggested that the $v \sin i$ distribution along the HB may bear the direct imprint of angular momentum transfer (from small-mass companions) during their previous RGB evolution. In particular, they have suggested that the high $v \sin i$ values found in several HB stars may be due to angular momentum transfer from a stellar or planetary companion, whose engulfment may have led to a spin-up of the primary star when the latter's external layers were expanded during the RGB phase. The added centrifugal acceleration to the RGB star's outermost layers could accordingly lead to an increase in the amount of mass lost by the RGB stars, thus leading to the formation of HB stars of lower mass, i.e., blue HB stars. Recently, Silvotti et al. (2007) found a giant planet orbiting V391 Pegasi, an extreme (blue) HB star, which lends some support to the planet engulfment scenario. However, no planets have hitherto been found in GCs, despite the fact that several surveys have been dedicated to identify planetary systems in GCs (Gilliland et al. 2000; Weldrake et al. 2005). Otherwise, the distributions of metallicity for stars with planets show a bias for metal-poor stars, due to the fact that the majority of detected planets have as host metal-rich stars (Santos et al. 2003; Santos et al. 2004; Fischer & Valenti 2005). Other studies have argued that the $v \sin i$ values found in HB stars may be a consequence of complex angular momentum transfer mechanisms operating between the external layers and the degenerate cores of the RGB stars (e.g., Pinsonneault et al. 1991; Sills & Pinsonneault 2000).

Mengel & Gross (1976) showed that a rapidly spinning RGB core may lead to a delay in the onset of the He flash, and thus to an extension of the RGB phase towards higher luminosities and lower temperatures – which could thus also lead to an increased mass loss and hence to bluer HB stars (see also Sweigart 1997a,b). Stellar rotation has thus been pointed out as a possible contributor to the so-called “second parameter” phenomenon – namely, the presence of GCs with similar metallicities but different color distributions along the HB (see Catalan 2009, for a recent review).

The “Grudahl jump” discontinuity (Grundahl et al. 1999), characterized by overluminous stars in blue passbands, most notably in Strömgren u and Johnson U , is also reflected upon the values of $v \sin i$ found in blue HB stars (Recio-Blanco et al. 2002). The overluminosity in u was shown by Grundahl et al. to be due to the fact that HB stars with $T_{\text{eff}} > 11,500 \text{ K}$ are strongly affected by radiative levitation and gravitational settling. The ensuing stellar winds (Vink & Cassisi 2002) and strong chemical gradients (Sills & Pinsonneault 2000) could help spin down these stars. Interestingly, Recio-Blanco et al. (2002) suggested that there is no evidence for a link between evolution away from the zero age HB (ZAHB) and the $v \sin i$ values in HB stars.

The main aim of the present study is to carry out an analysis of the evolutionary behavior of rotation velocity in metal-poor stars, in the field and in Galactic GCs alike, based on a thorough compilation of $v \sin i$ measurements from the literature. The stars in our sample are widely distributed across the HR diagram, from the main sequence to later evolutionary stages, such as the RGB and the HB. The paper is structured as follows: in §2 the main characteristics of the working sample are described. The main results are presented in §3. Our conclusions are drawn in §4. All data used in this work are presented

in Tables 3 and 4.

2. THE WORKING SAMPLE

For the purpose of this work we have compiled the $v \sin i$ values available in the literature for stars with $[\text{Fe}/\text{H}] \leq -0.5$ dex. The stars are located in the field and in some Galactic GCs. The sample of field stars was obtained from Kinman et al. (2000), Behr (2003b), Carney et al. (2003, 2008), and De Medeiros et al. (2006). These stars are located in the MS, RGB, and HB phases. On the other hand, the sample of stars in GCs is restricted to HB stars. The data were obtained from Peterson (1985), Peterson et al. (1995), Cohen & McCarthy (1997), Behr (2003a), and Recio-Blanco et al. (2004). Several blue HB stars in metal-poor GCs present $[\text{Fe}/\text{H}] > -0.5$ as a consequence of radiative levitation; we will discuss this further in §3.3. Some relevant properties of the selected stellar sample are indicated in Table 1.

Nine HB stars considered in Peterson (1985) belong to the GC M 4 (NGC 6121), which was observed using the echelle spectrograph with a spectral resolution $R \sim 23,000$ at the Multiple Mirror Telescope Observatory. The $v \sin i$ measurements were carried out using some Mg lines and a Fe II line, with typical errors in the $v \sin i$ values of 4 km s^{-1} .

The $v \sin i$ values listed by Peterson et al. (1995) were derived using the O I line triplet at $7771\text{--}7775 \text{ \AA}$. Their stellar sample contains HB stars in three GCs: M 3 (NGC 5272), M 13 (NGC 6205), and NGC 288. The spectra were obtained at medium resolution ($R \sim 20,000$), and were collected with the fiber-fed system “Nessie” with an echelle spectrograph at the 4 m telescope at Kitt Peak Observatory/NOAO. The typical errors in the $v \sin i$ measurements are 5.0, 3.2, and 6.0 km s^{-1} for the stars in M 3, M 13, and NGC 288, respectively.

Five blue HB stars in M 92 (NGC 6341) were analyzed by Cohen & McCarthy (1997). They used the HIRES spectrograph on the Keck I telescope atop Mauna Kea to obtain high resolution spectra for these stars ($R \sim 36,000$). Two methods were used to derive $v \sin i$. The first was a comparison of Gaussian line fits for isolated and unblended stars with similar profile measurements for the arc emission lines, varying the strength of the rotational broadening. The second one was a comparison between the profiles of strong absorption lines of Fe and Ti with the profile of a single Th-Ar arc emission line. We decided to use only the data based on the latter method, since it appears to be more reliable for fast rotating stars. The average error in the $v \sin i$ measurements is 3.8 km s^{-1} .

The $v \sin i$ values of blue HB stars measured by Kinman et al. (2000) were obtained from medium- ($R \sim 15,000$) and high-resolution spectra ($R \sim 30,000$ and $R \sim 40,000$), collected at the Kitt Peak 0.9 m coudé feed spectrograph and the CAT+CES (1.4 m Coudé Auxiliary Telescope + Coudé Echelle Spectrograph) combination at La Silla, Chile. In this work the rotational velocities were obtained using the FWHM of the Mg II line ($\lambda 4481$) and the fit of the profile Mg II lines of the observed spectra with the synthetic one. When both measurements are available for a star, we obtained the $v \sin i$ from the average between both values. These data may have important uncertainties, but unfortunately the associated measurement errors are not available.

The Recio-Blanco et al. (2002, 2004) data refer to four metal-poor Galactic GCs, namely NGC 2808, M 15 (NGC 7078), M 79 (NGC 1904), and M 80 (NGC 6093). The stellar spectra were obtained with high resolution ($R \sim$

TABLE 1
DATA CHARACTERISTICS AND REFERENCES

Author	# stars	Method used	Resolution	$\langle \text{Error} \rangle_{v \sin i}$
Perterson (1985)	9	Profile fitting	23,000	4.0 km s ⁻¹
Peterson et al. (1995)	63	O I triplet	20,000	3.2-6.0 km s ⁻¹
Cohen & McCarthy (1997)	5	Profile fitting	36,000	3.8 km s ⁻¹
Kinman et al. (2000)	28	Gaussian fitting	15,000	...
			30,000	...
			40,000	...
Recio-Blanco et al. (2002)	63	Cross-correlation	40,000	5.0 km s ⁻¹
			Behr (2003a)	74
Behr (2003b)	90	Profile fitting	45,000	3.0 km s ⁻¹
			60,000	
			Carney et al. (2003)	80
De Medeiros (2006)	99	Profile fitting	48,000	2.0 km s ⁻¹
			50,000	
Carney et al. (2008)	19	Fourier decomposition	120,000	1.0 km s ⁻¹

40,000) using UVES at the Kueyen-VLT. The values of $v \sin i$ for each star were obtained using the procedure described in Tonry & Davis (1979) and Melo, Pasquini, & De Medeiros (2001). The typical error in the computed $v \sin i$ is around 5 km s⁻¹. Most stars contained in this work do not have associated [Fe/H] measurements, but we were able to incorporate [Fe/H] values for some of the stars in M 79 based on the Fabian et al. (2005) study.

The stars in Behr (2003a) were observed with the HIRES-Keck spectrograph using a spectral resolution $R \sim 45,000$ and $R \sim 36,000$. To compute $v \sin i$ he used the minimum value of χ^2 for the fit between the metal absorption lines and Kurucz synthetic spectra. The stars belong to six Galactic GCs: NGC 288, M 3, M 13, M 15, M 68 (NGC 4590), and M 92. The typical error in $v \sin i$ is 3.0 km s⁻¹. Behr's (2003b) sample, in turn, contains field stars only. The stars were observed at high resolution ($R \sim 60,000$ and $R \sim 45,000$) using the Cassegrain echelle spectrograph on the McDonald Observatory 2.1 m Otto Struve Telescope and the HIRES-Keck spectrograph. The $v \sin i$ values were calculated using the same method as in Behr (2003a). The maximum error in the determination of $v \sin i$ is 3.0 km s⁻¹.

Carney et al. (2003) used field RGB and red HB stars, which were observed with the 1.5 m Wyeth reflector at the Oak Ridge Observatory in Harvard, Massachusetts. They also used the 1.5 m Tillinghats reflector and the Multiple Mirror Telescope atop Mount Hopkins, in Arizona. The $v \sin i$ values were derived from the comparison of observed rotational broadening with synthetic spectra, and the typical error in $v \sin i$ measurements ranges from 0.5 to 2.0 km s⁻¹.

The working sample in De Medeiros et al. (2006) is comprised of metal-poor field stars in three evolutionary stages, from the MS to the HB. The spectra were observed with high resolution ($R \sim 48,000$ and $R \sim 50,000$) at the FEROS spectrometer mounted on the ESO 1.5 m telescope, together with the CORALIE spectrometer mounted on the Euler Swiss 1.2 m telescope, both at La Silla, Chile. The $v \sin i$ values of the stellar sample were calculated by fitting the observed spectra with a synthetic one. They used metallic lines to compute $v \sin i$. Typical error on the $v \sin i$ measurements for their working sample is around 2 km s⁻¹.

The data compiled in Carney et al. (2008) corresponds to 12 metal-poor field RGB stars and 7 metal-poor field red HB

stars, which were observed using the Gecko spectrograph at the Canada-France-Hawaii Telescope (CFHT) with a typical $R \sim 120,000$. In this work the authors identified the $v \sin i$ and the macroturbulence component in the Doppler broadening in the line profiles using a Fourier analysis. The typical error in the $v \sin i$ measurements is ~ 1.0 km s⁻¹.

Some HB stars in GCs do not have measurements of their surface gravities and iron abundances. For some stars in the GCs M 3, M 15 and NGC 288 we compiled the surface gravities from Crocker et al. (1988) and Moehler et al. (1995). In order to have an estimation of the surface gravities for stars without any measurements in M 3, M 13, M 15, M 79, M 80, M 92, NGC 288, and NGC 2808, we used empirical (though approximate) relations between T_{eff} and $\log(g)$. More specifically, for the GCs M 3, M 13, M 79, and M 80, we used eq. (2) in Fabian et al. (2005), whereas for the GCs NGC 288 and NGC 2808 we used eq. (1) in Pace et al. (2006). For M 15 we used the values of $\log(g)$ found in Behr (2003a) to interpolate (or extrapolate) the surface gravities for stars in M 15. Otherwise, for those stars without [Fe/H] measurements, we assumed that the amount of heavy elements is equal to the characteristic abundances in the GC, which are presented in Table 2 (Harris 1996). Obviously we can only assume this for stars with $T_{\text{eff}} \leq 11,500$ K.

In Tables 3 and 4 we summarize the data for the field and GC stars analyzed in this paper, respectively. As we can see, several stars were analyzed in more than one study. For these stars we averaged the values of their physical and chemical parameters, as well as their measured rotational velocities, and we used these averaged values in our analysis. In Table 3 we also present some photometrical quantities for our field stars. The V magnitude and $(B-V)$ color were compiled from SIMBAD⁷, and the $(V-I)$ color comes from the Hipparcos catalog (Perryman et al. 1997 and references therein). References to the $v \sin i$ measurement sources are also included in this table. In Table 4 we present the apparent magnitude V and color index $(B-V)$. For the stars in M 79 the V values are based on measurements using the y passband of the Strömgren system, since V and y magnitudes are well known to be basically identical (Clem et al. 2004). We calculated the absolute magnitude M_V and the unreddened color $(B-V)_0$ provided in Table 4 using the distance modulus and reddening

⁷ <http://simbad.u-strasbg.fr/simbad/>

TABLE 2
CHEMICAL AND PHOTOMETRICAL PARAMETERS FOR
GALACTIC GCs

Cluster	[Fe/H]	M_V	$(m-M)_V$	$E(B-V)$
NGC 288	-1.24	-6.74	14.83	0.03
NGC 2808	-1.15	-9.39	15.59	0.22
M 3 (NGC 5272)	-1.57	-8.93	15.12	0.01
M 4 (NGC 6121)	-1.20	-7.20	12.83	0.36
M 13 (NGC 6205)	-1.54	-8.70	14.48	0.02
M 15 (NGC 7078)	-2.26	-9.17	15.37	0.10
M 68 (NGC 4590)	-2.02	-7.35	15.19	0.05
M 79 (NGC 1904)	-1.57	-7.86	15.59	0.01
M 80 (NGC 6093)	-1.75	-8.23	15.56	0.18
M 92 (NGC 6341)	-2.28	-8.20	14.64	0.02

values compiled in Harris (1996) for each GC (see Table 2).

In order to improve the analysis, we divided our stellar sample into different evolutionary stages, leading to a total of 51, 131, and 277 stars on the main sequence, the sub-giant branch (SGB) and RGB, and the HB, respectively. We note that in the RGB sample there are 14 confirmed binary systems (see table 5 in Carney et al. 2003 for details). The HB group was divided in two subgroups, the field HB group with 70 stars, and the HB in GCs group with 207 stars. Let us stress that there is an important difference between the resulting field and GC HB samples: while the field HB sample is comprised of red and blue HB stars (though with $T_{\text{eff}} < 11,500$ K), the GC HB sample is entirely comprised of blue HB stars.

3. RESULTS AND DISCUSSION

Figure 1 shows the distribution of $v \sin i$ along the HR diagram for metal-poor stars. This figure shows that most of these stars present low values of $v \sin i$, and that these slow rotators are located along all evolutionary stages, from the MS to the HB. There are several stars with high $v \sin i$, and those are mainly located on the HB. However, we can identify some fast rotators that are not on the HB, but which were rather catalogued as MS stars by Behr (2003b). We will discuss these stars in more detail in §3.1. Note also that the RGB stars present almost exclusively low values of $v \sin i$, with a single exception.

We have separated our sample into three different groups, where the stars are organized by iron abundance. We made this separation in order to identify possible systematic differences in the behavior of $v \sin i$ for the different metallicities considered here. The first group, FE1, is formed by 52 stars with $-1.0 < [\text{Fe}/\text{H}] \leq -0.5$; the second group, FE2, presents 236 stars with $-2.0 \leq [\text{Fe}/\text{H}] < -1.0$; and the last group, FE3, presents 130 stars with $[\text{Fe}/\text{H}] \leq -2.0$. There are also 19 HB stars with unknown metallicities and 22 metal-poor HB stars affected by radiative levitation ($-0.5 < [\text{Fe}/\text{H}] < +0.75$). We show the histograms of $v \sin i$ of groups FE1, FE2, and FE3 in Figure 2, where we can see that the distributions are very similar. In particular, the range in $v \sin i$ values is closely the same for all groups. Also, the fraction of stars contained in the interval $0.0 \leq v \sin i < 15.0 \text{ km s}^{-1}$ is 0.83, 0.84, and 0.80 for the groups FE1, FE2, and FE3, respectively. We stress that groups FE2 and FE3 present particularly similar $v \sin i$ distributions, with the histograms presenting closely the same shapes and peak locations; note that these two groups contain most of the stars in our sample. On the other hand, the distribution of $v \sin i$ for group FE1 presents a higher peak at $2.5 \leq v \sin i < 5.0 \text{ km s}^{-1}$ than do the other groups: indeed, the

fraction of stars in this $v \sin i$ interval is 0.56, 0.26, and 0.28 for FE1, FE2, and FE3, respectively. Figure 3 shows the values of surface gravities $\log(g)$ and $v \sin i$ for the same groups. This figure reveals that the differences in the $v \sin i$ distributions are related to the number of stars in the different evolutionary stages, the stars in the FE2 and FE3 groups covering all values of $\log(g)$ and being located in all evolutionary stages, whereas most of the stars contained in the FE1 group present high values of $\log(g)$ and are mainly located on the MS. However, we can note that there are a few FE1 stars located on the RGB and the HB, and that these evolved stars present the same rotational behavior as do the stars in groups FE2 and FE3 at a similar evolutionary stage. This suggests that metallicity is not an important parameter defining stellar rotation – or, at least, we do not identify important differences in the rotational behavior between the metallicity groups considered here. Certainly, more observations are required to analyze the behavior of the rotation in RGB and HB stars, especially over the metallicity range $-1.0 < [\text{Fe}/\text{H}] \leq -0.5$, in order to corroborate the suggested mild dependence of $v \sin i$ with $[\text{Fe}/\text{H}]$.

Note, on the other hand, that there are some observational biases in the available field star samples. Mainly, the observed stars with measurements of $v \sin i$ tend to be bright in the sky, and their parallaxes show that they are indeed found mainly in the solar neighborhood – which can be understood because, in order to obtain reliable measurements of $v \sin i$, high signal-to-noise ratio and medium-to-high spectral resolution are required. The low apparent magnitude is an observational constraint which can in principle also cause bias. In fact, the distribution of metallicities can be affected by choosing stars with low magnitudes; note, in particular, that the stars in our sample have mostly $V \leq 12$, and there are only two stars with $V \sim 14$. Although several works have been developed to search for differences in the rotational behavior as a function of position in the Milky Way (e.g., De Medeiros et al. 2000), there is no strong evidence showing important differences in the stellar rotation as a function of the Galactic latitude or the distance from the Galactic center. However, we stress the fact that the studies that have been carried out so far are focused on relatively bright stars. When future studies consider a representative sample both in magnitudes and Galactic positions, we should be in a position to derive stronger constraints on the behavior of $v \sin i$ as a function of position in our galaxy. We thus warn the reader that our study may suffer from such a source of bias, which however will only be possible to reliably quantify when significantly enlarged samples become available.

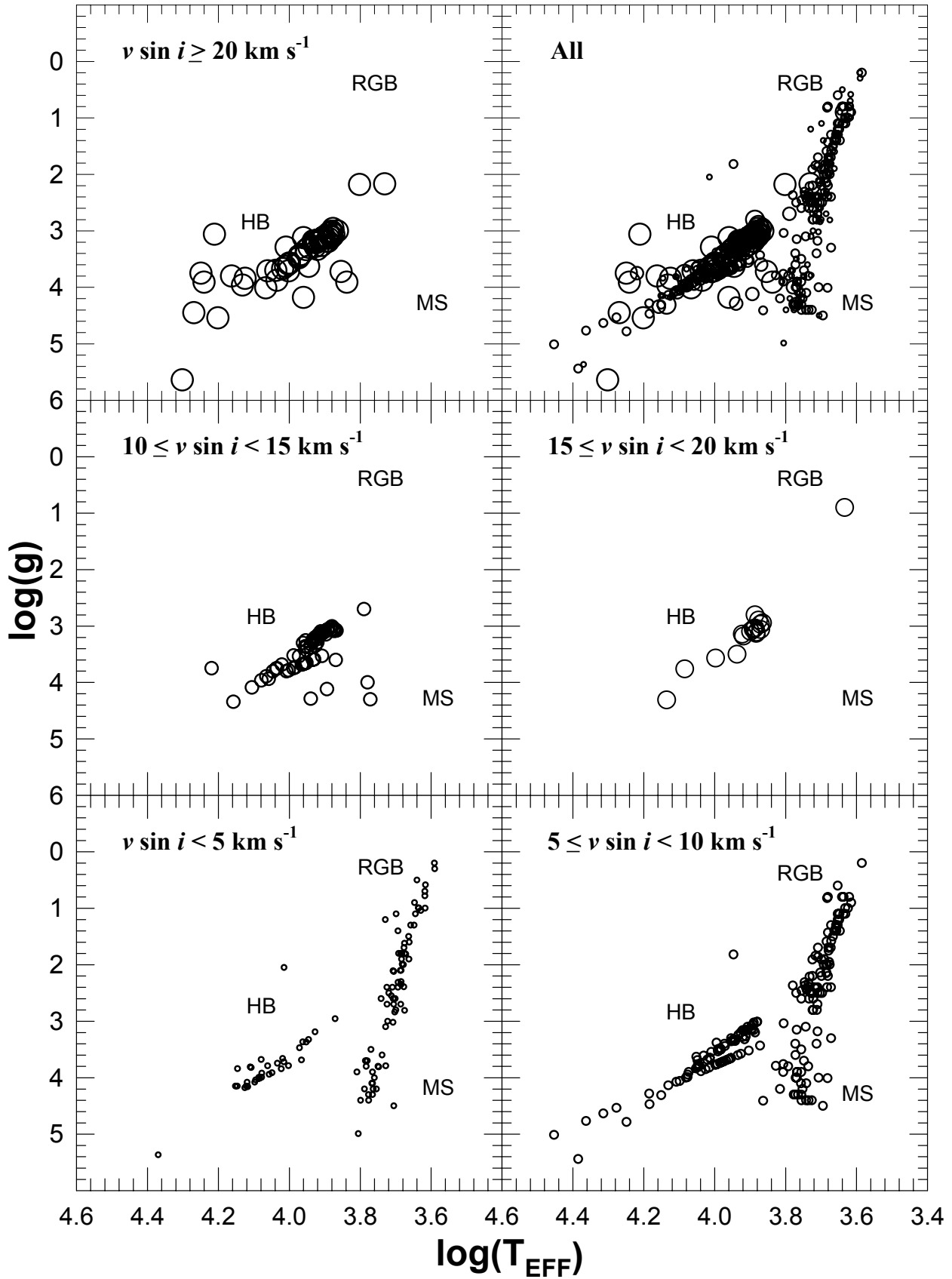


FIG. 1.— The distribution of $v \sin i$ on the HR diagram for the stars in our sample. The panels represent different $v \sin i$ intervals, as indicated. The main evolutionary stages are also schematically indicated. Note that slow rotators can be found throughout the HR diagram, whereas the fast rotators are found almost exclusively over a restricted range in HB temperatures.

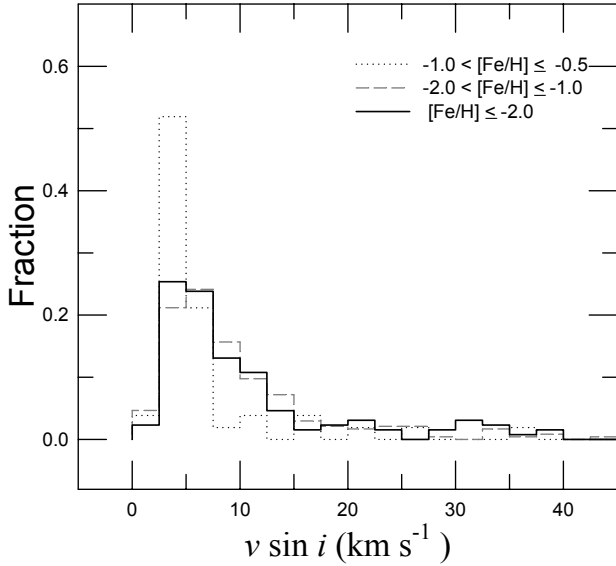


FIG. 2.— Histograms of $v \sin i$ as a function of $[\text{Fe}/\text{H}]$ for the stars in our stellar sample. Groups FE1, FE2, and FE3 are shown (see text). The $v \sin i$ distribution does not appear to present a significant dependence on metallicity.

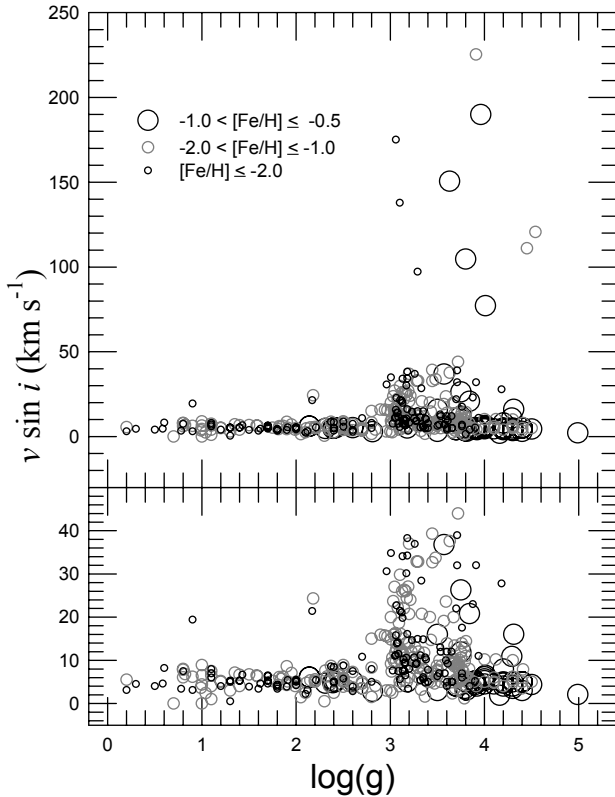


FIG. 3.— $v \sin i$ distribution as a function of surface gravity $\log(g)$ for different metallicity intervals. The lower panel represents a zoom around the low- $v \sin i$ region shown in the upper plot. The $v \sin i$ distribution for a given $\log(g)$ does not appear to show a significant dependence on metallicity.

3.1. Main Sequence and Turn-Off Stars

The distribution of $[\text{Fe}/\text{H}]$ for MS stars in the present sample is shown in Figure 4 (*upper left panel*). There are 51 MS and turn-off stars in our working sample, distributed across the three metallicity groups FE1, FE2, and FE3 described above according to the following percentages: 50.1%

(26 stars), 41.1% (21 stars) and 7.8% (4 stars), respectively. Figure 3 shows that the MS stars in the different metallicity groups present similar rotational behavior. This is especially clear for groups FE1 and FE2.

The $v \sin i$ distribution of our metal-poor MS stars shows that most of the hydrogen core burning stars are slow rotators (see Fig. 4, *left lower panel*). However, we also note that there are a few stars with high $v \sin i$ values. Figure 5 shows the projected rotational velocity $v \sin i$ as a function of $\log(T_{\text{eff}})$ (*upper panel*) and the corresponding cumulative $v \sin i$ distribution (*lower panel*). The *upper panel* in this figure shows that there is a clear relation between $v \sin i$ and T_{eff} , which may also be partly understood as a relation between $v \sin i$ and stellar mass. We can see clearly that the hotter (or more massive) MS stars present a spread in $v \sin i$ values, with values reaching up to a few hundred km s^{-1} . The cooler (or less massive) MS stars, on the other hand, present low $v \sin i$ values only. More specifically, 74.5% (38 stars) of them present $0.0 < v \sin i \leq 15.0 \text{ km s}^{-1}$, 7.8% (4 stars) present $15.0 < v \sin i \leq 50.0 \text{ km s}^{-1}$, and 17.7% (9 stars) present $v \sin i > 50.0 \text{ km s}^{-1}$.

Many studies have been conducted over the years in order to understand the rotational behavior of stars in the MS phase (e.g., Wilson 1966; Kraft 1967; Smith 1979; Soderblom 1983; Stauffer et al. 1984; Stauffer et al. 1985; Melo et al. 2001). These works found that the metal-rich MS stars can present high values of $v \sin i$, but these values are primarily linked with the stellar ages and masses. Skumanich (1972) and Pace & Pasquini (2004) found some observational laws to describe the evolution of the rotation velocity in low-mass stars, where we can see that the evolved metal-rich MS stars present low values of $v \sin i$. However, these studies were focused on metal-rich stars in the field and several open clusters, and no similar work has ever been conducted in the metal-poor regime. In this context, it is very important to verify whether the empirical laws discovered by the quoted authors remain valid at low metallicity.

Considering that the stars with high $v \sin i$ values all have $\log(T_{\text{eff}}) \geq 3.825$ (and are thus relatively massive), and assuming that the quoted observational laws describing the evolution of rotation velocities can be extrapolated to the metal-poor domain, this should imply that the fast rotating MS stars in our sample are predominantly young. Still, the possibility that these stars present older ages is also worth discussing. In fact, their position in the HR diagram may lead one to question the evolutionary stage assigned to these fast rotators. In this sense, if these stars belonged to the HB, we should definitely expect to find the chemical patterns characteristic of radiative levitation and gravitational diffusion, including supersolar $[\text{Fe}/\text{H}]$ values for stars with $T_{\text{eff}} > 11,500$ [$\log(T_{\text{eff}}) \geq 4.06$]. However, these stars are all metal-poor, thus rendering this possibility unlikely.

Another possibility is that some of these stars could be hypervelocity stars ejected from the Galactic center, since high rotation velocities have recently been measured for some such stars (López-Morales & Bonanos 2008). However, none of the stars in our sample appears to be a hypervelocity star. Perhaps a more realistic explanation could be that at least some of these stars are actually field blue straggler (BS) stars, particularly in view of the fact that at least some such stars are also fast rotators (e.g., Ryan et al. 2002). Such a possibility cannot be discarded, because the BSs present similar physical parameters as the hot MS stars in our sample.

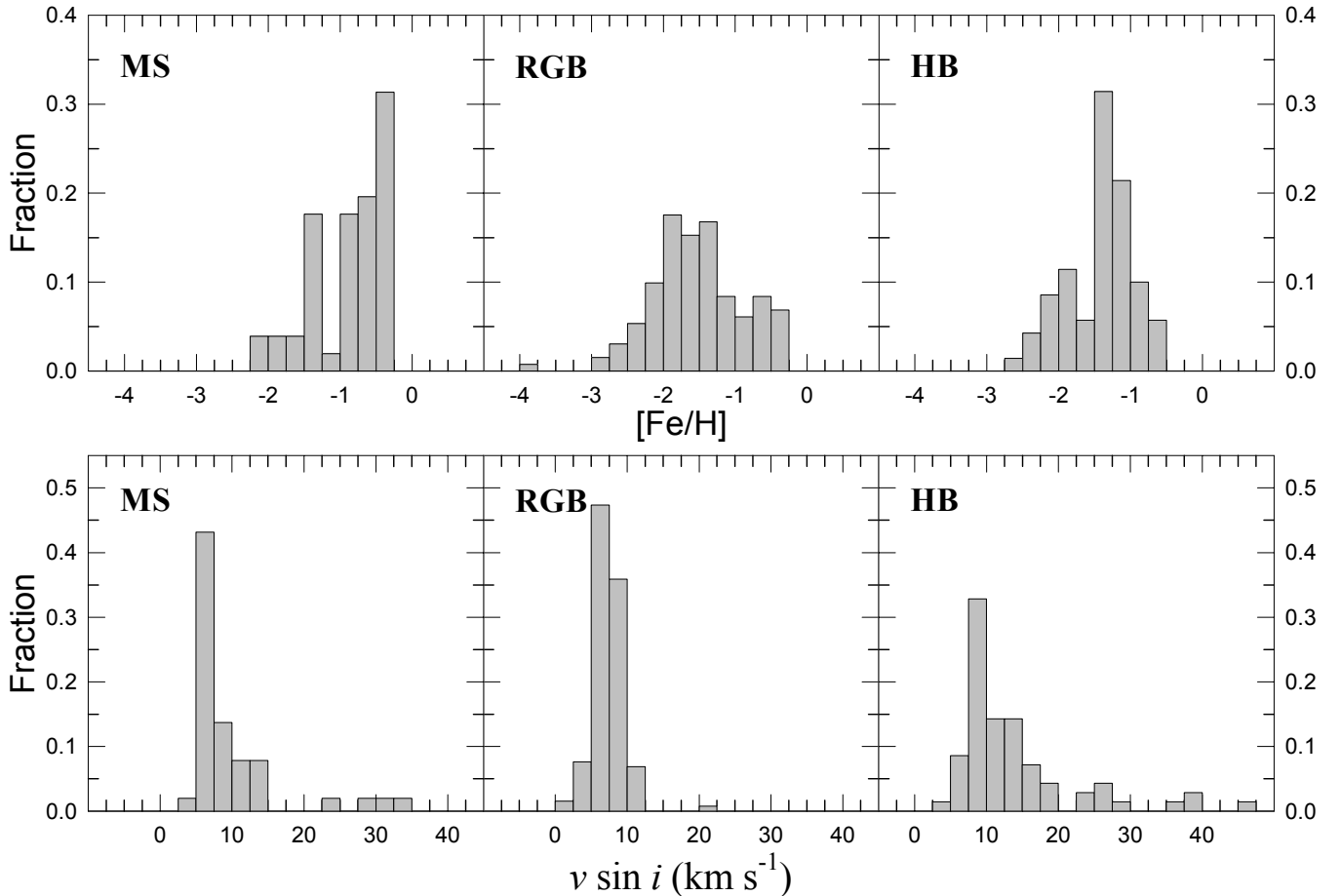


FIG. 4.— Histograms of $[Fe/H]$ (*upper panel*) and $v \sin i$ (*lower panel*) for field stars on the MS, the RGB, and the HB (from *left to right*). HB stars whose abundances are affected by radiative levitation are not included. There are clearly strong differences between the $v \sin i$ distributions for RGB and HB stars.

On the other hand, for those MS stars with $\log(T_{\text{eff}}) \leq 3.825$ (or less massive), the $v \sin i$ values are low. We would like to compare the values of $v \sin i$ for these stars with the values found in GCs. The average $v \sin i$ for field stars is $\langle v \sin i \rangle = 5.18 \pm 1.66 \text{ km s}^{-1}$. Lucatello & Gratton (2003) found in the GCs NGC 104 (47 Tuc), NGC 6397 and NGC 6752 an upper limit of $3.5 \pm 0.2 \text{ km s}^{-1}$ for the $v \sin i$ of turn-off stars (specifically, they found $4.0 \pm 0.4 \text{ km s}^{-1}$, $3.1 \pm 0.3 \text{ km s}^{-1}$, and $3.6 \pm 0.3 \text{ km s}^{-1}$ for 47 Tuc, NGC 6397, and NGC 6752, respectively). For our sample, the mean value of $v \sin i$ is higher than the upper limit found in the GCs. We note that this is not a strong evidence of differences or similarities in the rotational behavior of stars in field and clusters, because of the paucity of both samples. Nevertheless, if the Skumanich (1972) law can describe the rotation of the metal-poor stars, we note that the difference between the mean value found here and the mean value given by Lucatello & Gratton could result from a difference in ages for the stars in the field and in the GCs, since stars in GCs are generally older than those in the field. On the other hand, the positions of the stars of Lucatello & Gratton in the color-magnitude diagram show that the stars in NGC 6397 and NGC 6752 are on the turn-off (Gratton et al. 2001), while the stars in 47 Tuc are just above the turn-off point (Carretta et al. 2004). Interestingly, Melo et al. (2001) found that the stars just above the turn-off point in M 67 (NGC 2682) present a reduction in rotation velocities, with the stars below the turn-off presenting $v \sin i$ values al-

most 50% higher. The possibility cannot be excluded that age effects may also be present, since it has been suggested that 47 Tuc may be slightly younger than NGC 6397 or NGC 6752 (e.g., Gratton et al. 2003).

3.2. Sub-Giant and Red Giant Branch Stars

The *central upper panel* in Figure 4 shows that the $[Fe/H]$ distribution of the SGB and RGB stars considered in our stellar sample closely resembles a normal distribution. There are 131 stars in this stage, distributed into groups FE1, FE2, and FE3 in the following proportions, respectively: 15.3% (20 stars), 46.6% (61 stars), and 38.2% (50 stars).

The histogram of $v \sin i$ for SGB and RGB stars (see Fig. 4, *central lower panel*) shows that most of these stars with expanding photospheres are slow rotators. In Figure 6 we show $v \sin i$ as a function of effective temperature for these stars (*upper panel*), where we have included both single stars (open circles) and stars in confirmed binary systems (filled circles). Figure 6 also includes the recent measurements of $v \sin i$ in RGB stars by Carney et al. (2008), where we have included the single RGB stars (open inverted triangles) and the confirmed binary systems (filled inverted triangles). The cumulative $v \sin i$ distribution for all SGB and RGB stars is also presented in Figure 6 (*lower panel*). Most SGB and RGB stars present low $v \sin i$ values ($v \sin i \leq 15.0 \text{ km s}^{-1}$). The RGB stars in binary systems present similar rotational behavior, for a given T_{eff} , to the single RGB stars. There is a single binary system presenting high rotation (19.4 km s^{-1}), namely star

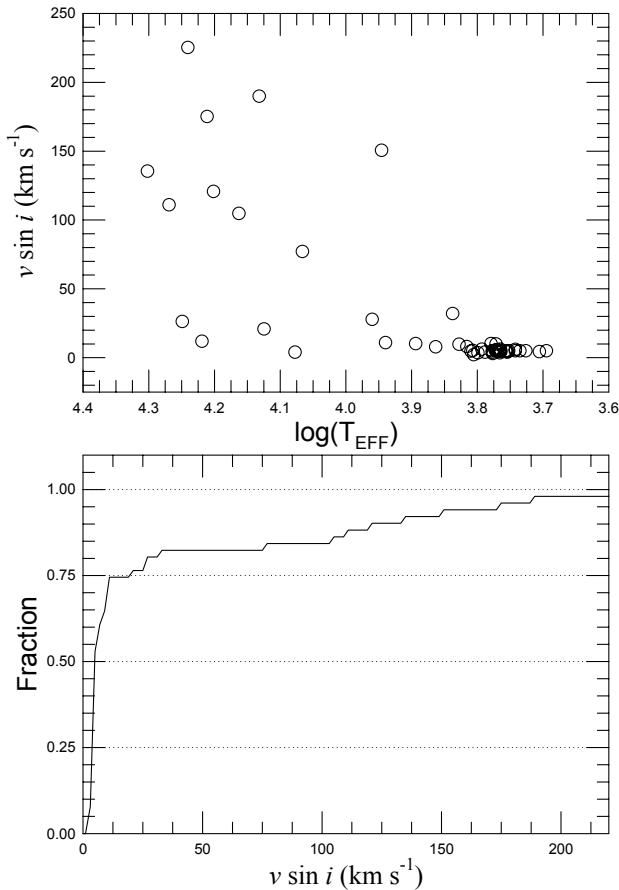


FIG. 5.— *Upper panel*: $v \sin i$ values for the field main sequence stars as a function of T_{eff} . *Lower panel*: cumulative $v \sin i$ distribution for MS stars.

CD-37°14010, which has an orbital eccentricity $e = 0.058$ and an orbital period $T = 62.55 d$ (Carney et al. 2003). These orbital parameters suggest that this star is synchronized, thus explaining its enhanced rotation.

Another important result is that the stars pass along the RGB with $v \sin i$ values that seem to remain practically constant (Fig. 6). This feature was also found in stars in the field and open clusters (Pasquini et al. 2000; Melo et al. 2001). Naturally, if these stars conserve angular momentum, the expansion in their radius should produce a reduction of the $v \sin i$ value at the surface. In addition, the rotation should slow down due to the angular momentum that is lost as the star loses mass during its approach of the RGB tip. However, the RGB stars in our sample do not show this feature, i.e., they do not slow down as they approach the RGB tip – as also reported by Carney et al. (2008). As a matter of fact, if one considers solely the Carney et al. (2008) sample, one is led to conclude that the stars arriving at the tip of the RGB may even present an *enhanced* rotation (see inverted triangles in Fig. 6). However, this enhancement does not become apparent when data from other studies are also incorporated, as can also be seen from Figure 6. More data for stars close to the RGB tip are needed to conclusively settle this issue.

The mean values of $v \sin i$ are also calculated for the single stars and the binary systems, and we found that these values are $\langle v \sin i \rangle = 4.79 \pm 1.75 \text{ km s}^{-1}$ and $\langle v \sin i \rangle = 6.24 \pm 4.35 \text{ km s}^{-1}$, respectively. When we do not take into account the CD-37°14010 star, the mean value of the binary system is $\langle v \sin i \rangle = 5.14 \pm 1.89 \text{ km s}^{-1}$. If the stars of Carney et al.

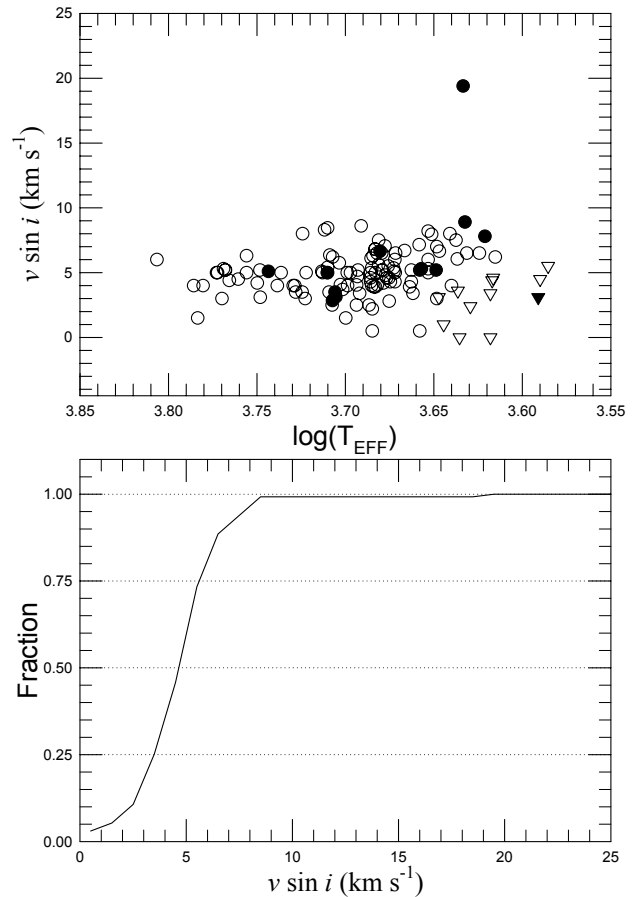


FIG. 6.— *Upper panel*: $v \sin i$ values for the field RGB stars as a function of T_{eff} . The open circles represent single RGB stars, whereas the filled black circles represent binary systems. Binary systems present a similar behavior as single RGB stars. The stars of Carney et al. (2008) are also presented, with the open triangles representing single RGB stars in their sample, and the filled black triangles representing binary systems studied by these authors. *Lower panel*: cumulative $v \sin i$ distribution for the RGB stars.

(2008) are not considered, we obtain $\langle v \sin i \rangle = 4.98 \pm 1.63 \text{ km s}^{-1}$ and $\langle v \sin i \rangle = 5.33 \pm 1.87 \text{ km s}^{-1}$ for the single stars and the binary systems (without the star CD-37°14010), respectively.

3.3. Horizontal Branch Stars

The *right upper panel* in Figure 4 shows the distribution of $[\text{Fe}/\text{H}]$ for the field HB stars. There are 70 stars in this stage in our sample. 5.7% (4 stars), 68.6% (48 stars), and 25.7% (18 stars) are the percentages of HB stars in groups FE1, FE2, and FE3, respectively.

The histogram of $v \sin i$ for field HB stars (see Fig. 4, *right lower panel*) shows that the helium core burning stars cannot be generally considered slow rotators, because they present a spread of $v \sin i$ values. In spite of the fact that HB stars present a narrow range in masses (from about 0.5 to $1.0 M_{\odot}$), they show $v \sin i$ values up to several tens of km s^{-1} . This characteristic cannot be straightforwardly explained in terms of canonical stellar evolution models, because their ancestors (RGB stars and low-mass MS stars), as we noted in previous sections, are mainly slow rotators.

In order to observe the differences or similarities in the behavior of the rotation between HB stars in the field and GCs, we have compared the values for field stars with those for stars in the GCs NGC 288, NGC 2808, M 3, M 4, M 13,

M 15, M 68, M 79, M 80, and M 92. For those stars without individual iron abundances and $T_{\text{eff}} < 11,500$ K, we assume the typical GC values (see Table 2). The HB stars in M 4 do not present T_{eff} measurements, but their $(B-V)$ colors point to $T_{\text{eff}} < 11,500$ K. 1.0% (2 stars), 51.2% (106 stars), and 28.0% (58 stars) are the percentages of stars in groups FE1, FE2 and FE3, respectively. 10.6% (22 stars) present enhanced metallicity ($[\text{Fe}/\text{H}] > -0.5$), due to radiative levitation, and 9.2% (19 stars) do not have $[\text{Fe}/\text{H}]$ measurements and are hotter than the Grundahl jump, with $T_{\text{eff}} > 11,500$ K.

Figure 7 shows the histograms of $[\text{Fe}/\text{H}]$, $v \sin i$ and T_{eff} for stars in the field and GCs contained in our sample. Apart from the discreet nature of the GC $[\text{Fe}/\text{H}]$ distribution, there are no outstanding differences between the histograms for the field and GC samples. In addition, the GC distribution clearly reveals the presence of stars with enhanced iron abundances, as produced by the effects of metal levitation. As previously noted, HB stars with $T_{\text{eff}} \geq 11,500$ K are affected by radiative levitation and gravitational settling, thus the amount of iron and other heavy elements in their atmospheres is strongly enhanced (e.g., Grundahl et al. 1999; Moehler et al. 1999, 2000; Fabbian et al. 2005; Pace et al. 2006; and references therein). However, this effect cannot be noted among the field stars in our sample, because there are important differences in the T_{eff} distribution of both samples (see Fig. 7, *right panel*). Our sample of field stars is comprised of blue and red HB stars, and no stars present $T_{\text{eff}} > 10,500$ K, whereas the stars in the GC sample are blue HB stars only. To be sure, Behr (2003b) does list a few HB stars with higher temperatures, but they all have, probably as a consequence of radiative levitation, high metallicities. Since we are unable to infer these stars' original metallicities, we do not include them in our sample of field HB stars. In the case of GCs, the original metallicities of the HB stars showing radiative levitation effects can be easily determined, since they should – at least in monometallic clusters – be basically identical to those of stars in the same GCs that are not affected by radiative levitation.

Figure 8 shows the rotational velocities of the HB stars as a function of temperature and $[\text{Fe}/\text{H}]$. We can see three different groups, characterized by different distributions in $v \sin i$, $[\text{Fe}/\text{H}]$, and T_{eff} . We can identify these groups as the hot HB (i.e., HB stars hotter than the Grundahl jump), the blue HB (cooler than the jump), and the red HB. The hot HB stars present $T_{\text{eff}} \geq 11,500$ K and high values of $[\text{Fe}/\text{H}]$ (again due to radiative levitation). The blue HB stars present $7200 < T_{\text{eff}} < 11,500$ K, and the red HB stars have T_{eff} lower than 6300 K. Also shown is the instability strip, where the RR Lyrae stars are located. Figure 9 presents the values of $v \sin i$ as a function of T_{eff} (*upper panel*) and the cumulative $v \sin i$ distribution (*lower panel*) for the different groups of HB stars.

As proposed by Vink & Cassisi (2002), hot HB stars may lose mass, and such mass loss by stellar winds could also lead to a loss in angular momentum and thus a reduction in rotation velocities, thus explaining their low rotation velocities (see Fig. 8) of the HB stars hotter than the Grundahl jump (Sweigart 2002). Also, the strong element gradients in the atmospheres of these stars can inhibit angular momentum transport, thus also preventing these stars from becoming fast rotators, even if they are able to preserve a rapidly rotating core (Sills & Pinsonneault 2000). On the other hand, the stellar wind is predicted to become very weak in stars with $T_{\text{eff}} < 10000$ K. Indeed, in Figure 9 we can see that the values of $v \sin i$ for the blue HB stars tend to be higher when

$T_{\text{eff}} < 10000$ K, whereas the stars with $T_{\text{eff}} > 10000$ K present low $v \sin i$ values. Figure 9 also shows that the red HB stars are, mainly, slow rotators, thus suggesting an overall dependence of $v \sin i$ with T_{eff} (Carney et al. 2008).

Note that there are two stars classified as HB stars with $v \sin i$ values much higher than for the other fast HB rotators, namely BD+01° 0514 and BD+30° 2355, which present $v \sin i = 137.9 \text{ km s}^{-1}$ and 97.3 km s^{-1} , respectively. Behr (2003b) suggested that BD+01° 0514 is an RR Lyrae star, but to the best of our knowledge a variability analysis is not yet available for this star; additionally, RR Lyrae stars are known to be slow rotators (Peterson et al. 1996). BD+30° 2355 was, in turn, catalogued by Behr as a post-HB star. In view of their atypical rotation velocities, we suggest that neither of these stars is an HB or post-HB star, being more likely MS stars. Until this issue is resolved, these stars will not be considered in the following analysis.

We analyze the $v \sin i$ distribution of the blue (stars with $7200 < T_{\text{eff}} < 11,500$ K in the field and the GCs) and red groups of HB stars (see *lower panel* in Figure 9). In these groups we found $\langle v \sin i \rangle = 11.46 \pm 8.63, 12.81 \pm 8.63, 7.55 \pm 4.38 \text{ km s}^{-1}$ for blue HB stars in the field and the GCs, and red HB stars in the field, respectively. Specifically we found $\langle v \sin i \rangle_{\text{FE1}} = 16.03 \pm 14.69 \text{ km s}^{-1}$, $\langle v \sin i \rangle_{\text{FE2}} = 11.91 \pm 9.07 \text{ km s}^{-1}$ and $\langle v \sin i \rangle_{\text{FE3}} = 8.96 \pm 4.39 \text{ km s}^{-1}$ for blue HB in the field, $\langle v \sin i \rangle_{\text{FE2}} = 12.22 \pm 7.99 \text{ km s}^{-1}$ and $\langle v \sin i \rangle_{\text{FE3}} = 14.45 \pm 9.70 \text{ km s}^{-1}$ for blue HB in the GCs (no blue HB stars in FE1 group), and $\langle v \sin i \rangle_{\text{FE1}} = 5.65 \pm 0.64 \text{ km s}^{-1}$, $\langle v \sin i \rangle_{\text{FE2}} = 7.44 \pm 4.27 \text{ km s}^{-1}$ and $\langle v \sin i \rangle_{\text{FE3}} = 8.17 \pm 5.14 \text{ km s}^{-1}$ for red HB in the field. We can note that the mean values of $v \sin i$ for the blue HB star groups are very similar. The cumulative $v \sin i$ distributions reveal differences between the field and the GCs. However, this is not a strong result, and we should also keep in mind the relative paucity of the field star sample, with only 36 blue HB stars. We can also see that red and blue HB stars present different distributions, with the red HB stars presenting lower $v \sin i$ than the blue ones. We have applied the Kolmogorov–Smirnov (KS) test on the distributions of $v \sin i$ of blue HB stars (field stars and stars in GCs). We found that the maximum distance between both distributions is $D_{\text{max}} = 0.166$ and the probability that both distributions come from the same parent distribution is $P_{\text{KS}} = 94.5\%$, thus suggesting that the environment has not played a strong role in shaping the overall rotation distribution for HB stars (Behr 2003b). However, this does not rule out the possibility that, for some individual GCs, the rotation behavior has been markedly different than for field HB stars and for other GCs alike.

A very interesting property that is shared between blue HB stars in the field and in GCs is that in both groups the fraction of fast rotators is similar: approximately 31% and 25% of the blue HB stars have rotation velocities $v \sin i > 15.0 \text{ km s}^{-1}$ in the field and the GCs, respectively. We would like to remind the reader that the differences in the $[\text{Fe}/\text{H}]$ distributions between field and GC stars do not affect the corresponding $v \sin i$ distribution (see Fig. 7, *center panel*). On the other hand, the $v \sin i$ distribution of red HB stars is again markedly different from the distributions for the hot and blue HB stars, with the amount of fast rotators being only about 6% (but again we remark that the number of stars in the red HB sample is quite small). Obviously, observations of enlarged

samples will be needed to understand the behavior of rotation as a function of temperature along the HB. In this sense, it would be very interesting to derive rotation velocities for a large sample of RR Lyrae stars, in a temperature regime intermediate between the red and blue HB stars, but for which there is very little data currently available, suggesting however little or no rotation (e.g., Peterson et al. 1996).

Recio-Blanco et al. (2002) suggested that there is no correlation between the value of $v \sin i$ and the evolutionary stage on the HB. If confirmed, this would have important implications for our understanding of angular momentum evolution in HB stars, since most theoretical studies suggest that angular momentum loss and transport should be important in explaining the lack of fast rotators among stars hotter than the Grundahl jump, and likewise possibly their presence among blue HB stars cooler than this limit (e.g., Sills & Pinsonneault 2000; Sweigart 2002).

In order to analyze this suggestion, we have obtained, from different sources in the literature, the Johnson and Strömgren photometries for the stars with $v \sin i$ measurements in the GCs NGC 288, M 3 (NGC 5272), M 4 (NGC 6121), M 13 (NGC 6205), M 15 (NGC 7078), M 68 (NGC 4590), M 79 (NGC 1904), and M 92 (NGC 6341) (see table 4). We have derived the absolute magnitude in both photometric systems using the distance modules and reddening values compiled in Harris (1996). For the case of M 79, the absolute magnitude u and the unreddened colors $(u-y)_0$ in the Strömgren system were calculated using a $(m-M)_u = 15.6$ and $E(u-y) = 1.89E(B-V)$ (Crawford & Mandwewala 1976; Clem et al. 2004). We have transformed the evolutionary tracks and ZAHB sequences to the observational planes following the same procedures already described in Catelan et al. (2004) and Cortés & Catelan (2008). The evolutionary models used in the present study are the same as those computed by Catelan et al. (1998) and Sweigart & Catelan (1998). We have chosen the evolutionary tracks for different masses with metal abundances $Z = 0.0020$, 0.0010 , and 0.0005 (with MS helium abundance $Y_{\text{MS}} = 23\%$), since these values of Z adequately cover the metallicities of the GCs considered in our analysis. To transform these Z values into $[\text{Fe}/\text{H}]$, we have used equation (2) in Cortés & Catelan (2008), based on the scaling relation of Salaris et al. (1993) for an $[\alpha/\text{Fe}] = 0.3$, as typically found among halo stars (e.g., Pritzl et al. 2005 and references therein). Specifically, the evolutionary tracks with $Z = 0.0020$ ⁸ were used for the GCs NGC 288 and M4, the evolutionary tracks with $Z = 0.0010$ ⁹ for the GCs M 3, M 13 and M 79, and the evolutionary tracks with $Z = 0.0005$ ¹⁰ for the GCs M 92, M 15 and M 68. No attempt was made to properly model the stars hotter than the Grundahl jump at 11,500 K; the reader is thus warned that these models cannot be used to reliably describe the u -band magnitudes in particular of these stars (Grundahl et al. 1999).

Figure 10 shows the stars with measurements of $v \sin i$ in the different GCs, with the ZAHBs, TAHBs (terminal-age HBs, or helium core exhaustion locus), and the referred evolutionary tracks overplotted. We can see that there is no strong evidence that $v \sin i$ is linked with the evolutionary stage of the stars. Note, in particular, in several clusters, perhaps

most notably M13 and M92, we clearly find stars with high $v \sin i$ values very close to the ZAHB. Conversely, in several clusters we can also see slow rotators close to the ZAHB. This suggests that either these stars arrived at the ZAHB displaying rotation rates very similar to their current values, or else that angular momentum loss and redistribution may operate extremely fast once the stars reach the ZAHB.

In summary, we find that the values of $v \sin i$ for the HB stars are not correlated with the evolutionary distance from the ZAHB. However, enlarged samples of low-metallicity HB stars with accurately measured $v \sin i$ values are needed to put this result on a firmer footing.

4. CONCLUSIONS

In this paper, we have performed a careful compilation of $v \sin i$ values for metal-poor stars ($[\text{Fe}/\text{H}] < -0.5$) covering different evolutionary stages (MS, RGB, HB) from the literature. Our sample includes stars both in the field and in Galactic GCs. We also gathered metallicity and photometric data for these stars, and present all data in the form of extensive tabulations. We have conducted a preliminary analysis of these data, and our main conclusions are as follows.

The distribution of $v \sin i$ in the H-R diagram shows that the slow rotators are distributed in all evolutionary stages, from the MS to the HB. The fast rotators are concentrated in the HB, suggesting that the HB stars somehow acquired angular momentum in the previous phase (the RGB), or else that RGB stars preserved rapidly spinning cores and were later, either during the pre-ZAHB phase or on the HB proper, able to transfer angular momentum to the stellar surface. However, an analysis of evolutionary differences in $v \sin i$ values along the HB phase for eight different GCs reveals little or no dependence of $v \sin i$ on evolutionary phase, thus suggesting that any angular momentum transport or losses in the HB phase must either operate very quickly close to the ZAHB, or be very inefficient during the HB phase.

HB stars in the field and in GCs do not reveal important differences in their rotational behavior, thus suggesting that the environment does not affect the rotation behavior of these stars in an important way. However, we cannot rule out the possibility that some individual GCs will have a peculiar stellar rotation behavior, driven by environmental effects. In addition, sample sizes remain relatively small, and it would certainly be important to derive $v \sin i$ for enlarged samples of stars, in the field and in GCs alike, to put these results on a firmer footing. It would particularly interesting to derive $v \sin i$ for a large sample of RR Lyrae stars, for which very few measurements are currently available, and yet there is a puzzling indication of very little (or no) rotation (e.g., Peterson et al. 1996).

We also find that, while our field and GC samples have markedly different metallicity distributions, such differences are not reflected upon marked differences in their corresponding $v \sin i$ distributions. It thus appears that metallicity is not a relevant parameter affecting the overall $v \sin i$ distribution, at least in the low-metallicity regime studied in this work.

RGB stars in the Carney et al. (2008) sample reveal some intriguing evidence of spinning up as they approach the RGB tip. However, when we incorporate data for bright RGB stars from other sources, we do not find any significant variation in $v \sin i$ with evolutionary stage along the RGB.

This work has been supported by continuous grants from the CAPES, CNPq and FAPERN Brazilian agencies. We are

⁸ The masses of the evolutionary tracks for $Z = 0.0020$ are 0.500, 0.510, 0.520, 0.530, 0.540, 0.550, 0.560, 0.580, 0.600, and 0.620 M_{\odot} .

⁹ The masses of the evolutionary tracks for $Z = 0.0010$ are 0.495, 0.497, 0.506, 0.515, 0.527, 0.542, 0.558, 0.575, 0.589, 0.604, 0.616, and 0.630 M_{\odot} .

¹⁰ The masses of the evolutionary tracks for $Z = 0.0005$ are 0.498, 0.499, 0.501, 0.508, 0.519, 0.531, 0.565, 0.600, 0.630, 0.660, and 0.693 M_{\odot} .

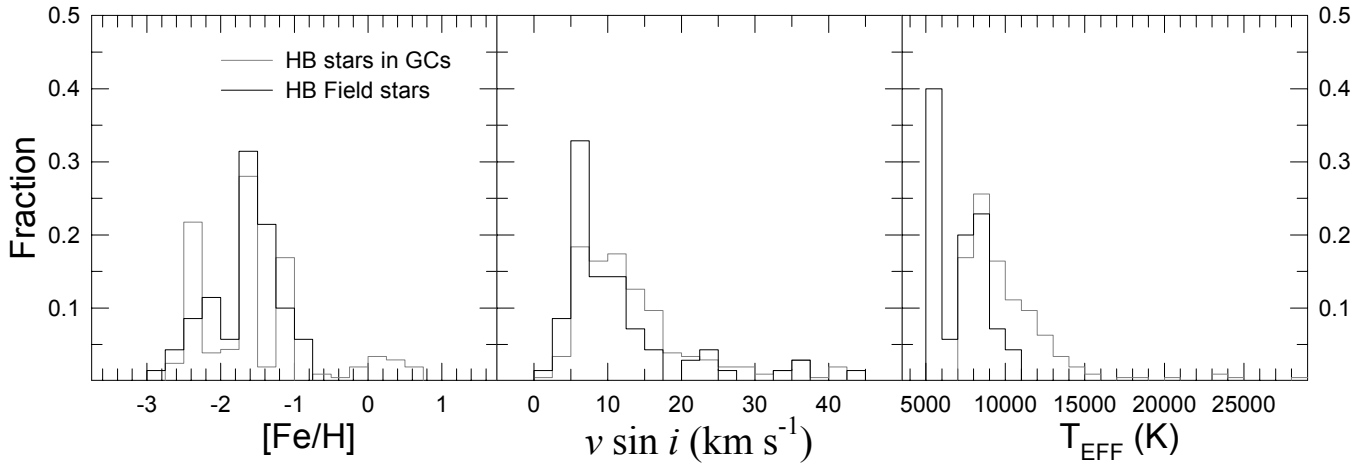


FIG. 7.— Histograms of $[\text{Fe}/\text{H}]$, $v \sin i$ and T_{eff} for horizontal branch (HB) stars (from left to right panels). Field HB stars are indicated by black lines, and HB stars in GCs by gray lines. While the $[\text{Fe}/\text{H}]$ histograms are very different, their $v \sin i$ distributions look very similar (see Fig. 8).

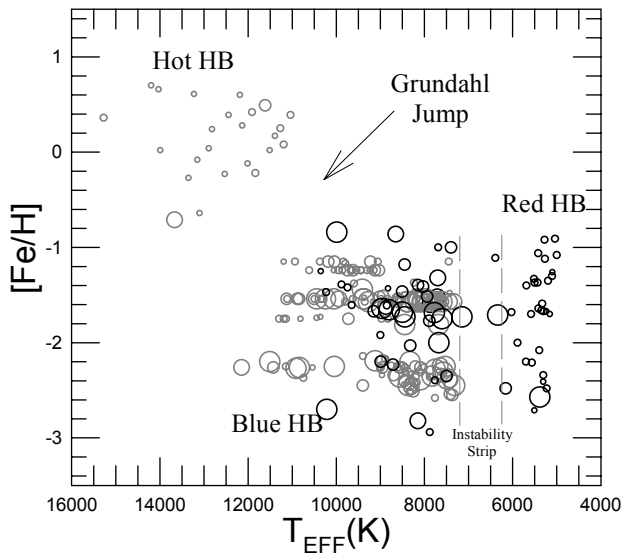


FIG. 8.— $v \sin i$ values for the HB stars as a function of metallicity and T_{eff} . As in Figure 1, the symbols represent different intervals of $v \sin i$. Field HB stars are presented with black open symbols, whereas HB stars in Galactic GCs are shown as gray open symbols. The different groups of HB stars (hot HB, blue HB, red HB) and the discontinuity in $v \sin i$ values and $[\text{Fe}/\text{H}]$, produced by the Grundahl jump, are readily apparent.

particularly grateful to CONICYT and CNPq for CONICYT-CNPq PCCI grant 018/DRI/061. M.C. thanks the John Simon Guggenheim Memorial Foundation for a Guggenheim Fellowship.

REFERENCES

- Behr, B. B., Djorgovski, S. G., Cohen, J. G., McCarthy, J. K., Côté, P., Piotto, G., & Zoccali, M. 2000a, *ApJ*, 528, 849
- Behr, B. B., Cohen, J. G., & McCarthy, J. K. 2000b, *ApJ*, 531, 37
- Behr, B. B. 2003a, *ApJS*, 149, 67
- Behr, B. B. 2003b, *ApJS*, 149, 101
- Carney, B. W., Latham, D. W., Stefanik, R. P., Laird, J. B., & Morse, J. A. 2003, *AJ*, 125, 293
- Carney, B. W., Gray, D. F., Yong, D., Latham, D. W., Manset, N., Zelman, R., & Laird, J. B. 2008, *AJ*, 135, 892
- Carretta, E., Gratton, R. G., Bragaglia, A., Bonifacio, P., & Pasquini, L. 2004, *A&A*, 416, 925
- Catelan, M. 2009, *Ap&SS*, 320, 261
- Catelan, M., Borissova, J., Sweigart, A. V., & Spassova, N. 1998, *ApJ*, 494, 265
- Catelan, M., Pritzl, B. J., & Smith, H. A. 2004, *ApJS*, 154, 633
- Clem, J. L., Vandenberg, D. A., Grundahl, F., & Bell, R. A. 2004, *AJ*, 127, 1227
- Cohen, J. G., & McCarthy, J. K. 1997, *AJ*, 113, 1353
- Cortés, C., & Catelan, M. 2008, *ApJS*, 177, 362
- Crawford, D. L., & Mandwewala, N. 1976, *PASP*, 88, 917
- Crocker, D. A., Rood, R. T., & O'Connell, R. W. 1988, *ApJ*, 332, 236
- De Medeiros, J. R., Carvalho, J. C., Soares, B. B., Da Rocha, C., & Maia, M. R. G. 2000, *A&A*, 358, 113
- De Medeiros, J. R., Silva, J. R. P., Do Nascimento, J. D., Jr., Canto Martins, B. L., da Silva, L., Melo, C., & Burnet, M. 2006, *A&A*, 458, 895
- Fabbian, D., Recio-Blanco, A., Gratton, R. G., & Piotto, G. 2005, *A&A*, 434, 235
- Fischer, D. A., & Valenti, J. 2005, *ApJ*, 622, 1102
- Gilliland, R. L., et al. 2000, *ApJ*, 545, L47
- Gratton, R. G., et al. 2001, *A&A*, 369, 87
- Gratton, R. G., Bragaglia, A., Carretta, E., Clementini, G., Desidera, S., Grundahl, F., & Lucatello, S. 2003, *A&A*, 408, 529
- Grundahl, F., Catelan, M., Landsman, W. B., Stetson, P. B., & Andersen, M. I. 1999, *ApJ*, 524, 242
- Harris, W. E. 1996, *AJ*, 112, 1487
- Kinman, T., Castelli, F., Cacciari, C., Bragaglia, A., Harmer, D., & Valdes, F. 2000, *A&A*, 364, 102
- Kraft, R. P. 1967, *ApJ*, 150, 551
- López-Morales, M., & Bonanos, A. 2008, *ApJ*, 685, L47
- Lucatello, S., & Gratton, R. G. 2003, *A&A*, 406, 691
- Melo, C. H. F., Pasquini, L., & De Medeiros, J. R. 2001, *A&A*, 375, 851
- Mengel, J. G., & Gross, P. G. 1976, *Ap&SS*, 41, 407

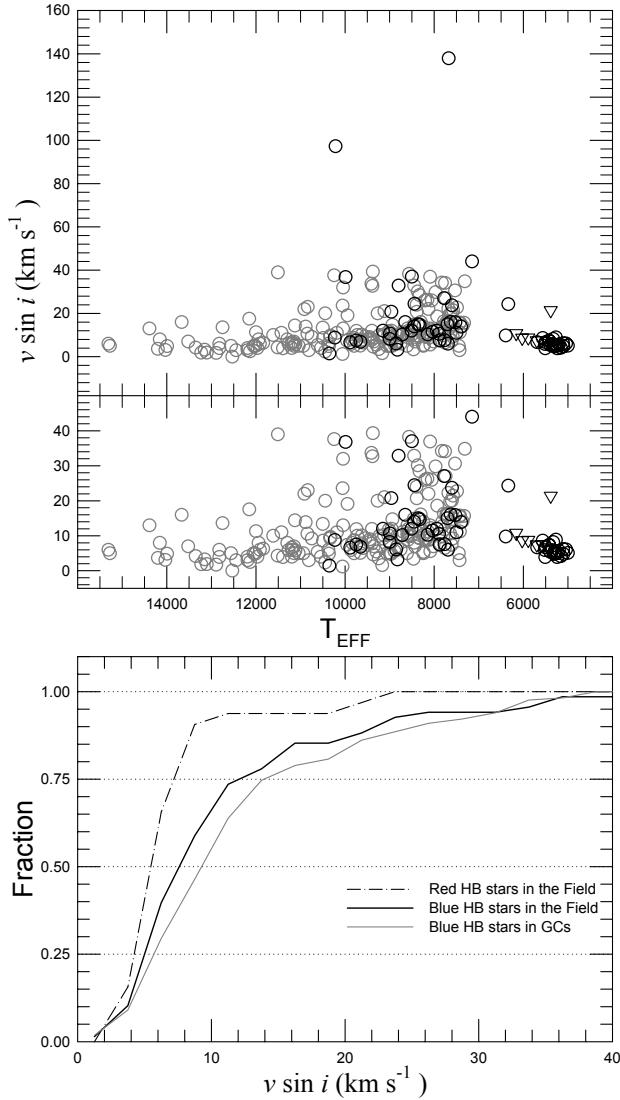


FIG. 9.— The *upper panel* shows $v \sin i$ as a function of T_{eff} for HB stars. Black circles represent field HB stars, gray circles the HB stars in Galactic GCs, and the inverted triangles the field red HB stars. The *lower panel* shows the corresponding cumulative $v \sin i$ distribution, where the two stars with unusually high rotation velocities ($v \sin i \gtrsim 100 \text{ km s}^{-1}$) were not included; see text). The solid gray line represents the distribution of blue HB stars in GCs, the solid black line represents the distribution of blue HB stars in the field, and the dash-dotted line represents the distribution of field red HB stars.

- Moehler, S., Heber, U., & de Boer, K. S. 1995, *A&A*, 294, 65
 Moehler, S., Sweigart, A. V., Landsman, W. B., Heber, U., & Catelan, M. 1999, *A&A*, 346, L1
 Moehler, S., Sweigart, A. V., Landsman, W. B., & Heber, U. 2000, *A&A*, 360, 120
 Pasquini, L., de Medeiros, J. R., & Girardi, L. 2000, *A&A*, 361, 1011
 Pace, G., & Pasquini, L. 2004, *A&A*, 426, 1021
 Pace, G., Recio-Blanco, A., Piotto, G., & Momany, Y. 2006, *A&A*, 452, 493
 Perryman, M. A. C., & ESA 1997, *ESA Special Publication*, 1200,
 Peterson, R. C. 1983, *ApJ*, 275, 737
 Peterson, R. C. 1985a, *ApJ*, 289, 320
 Peterson, R. C. 1985b, *ApJ*, 294, 35
 Peterson, R. C., Rood, R. T., & Crocker, D. A. 1995, *ApJ*, 453, 214
 Peterson, R. C., Carney, B. W., & Latham, D. W. 1996, *ApJ*, 465, L47
 Pinsonneault, M. H., Deliyannis, C. P., & Demarque, P. 1991, *ApJ*, 367, 239
 Pritzl, B. J., Venn, K. A., & Irwin, M. 2005, *AJ*, 130, 2140
 Recio-Blanco, A., Piotto, G., Aparicio, A., & Renzini, A. 2002, *ApJ*, 572, 71
 Recio-Blanco, A., Piotto, G., Aparicio, A., & Renzini, A. 2004, *A&A*, 417, 597
 Ryan, S. G., Gregory, S. G., Kolb, U., Beers, T. C., & Kajino, T. 2002, *ApJ*, 571, 501
 Salaris, M., Chieffi, A., & Straniero, O. 1993, *ApJ*, 414, 580
 Santos, N. C., Israelian, G., Mayor, M., Rebolo, R., & Udry, S. 2003, *A&A*, 398, 363
 Santos, N. C., Israelian, G., & Mayor, M. 2004, *A&A*, 415, 1153
 Skumanich, A. 1972, *ApJ*, 171, 565
 Sills, A., & Pinsonneault, M. H. 2000, *ApJ*, 540, 489
 Silvotti, R., et al. 2007, *Nature*, 449, 189
 Smith, M. A. 1979, *PASP*, 91, 737
 Soderblom, D. R. 1983, *ApJS*, 53, 1
 Soker, N. 1998, *AJ*, 116, 1308
 Soker, N., & Harpaz, A. 2000, *MNRAS*, 317, 861
 Stauffer, J. R., Hartmann, L., Soderblom, D. R., & Burnham, N. 1984, *ApJ*, 280, 202
 Stauffer, J. R., Hartmann, L. W., Burnham, J. N., & Jones, B. F. 1985, *ApJ*, 289, 247
 Sweigart, A. V. 1997a, *ApJ*, 474, L23
 Sweigart, A. V. 1997b, *The Third Conference on Faint Blue Stars*, 3
 Sweigart, A. V., & Catelan, M. 1998, *ApJ*, 501, L63
 Sweigart, A. V. 2002, *Highlights of Astronomy*, 12, 292
 Tonry, J., & Davis, M. 1979, *AJ*, 84, 1511
 van Leeuwen, F. 2007, *A&A*, 474, 653
 Vink, J. S., & Cassisi, S. 2002, *A&A*, 392, 553
 Weldrake, D. T. F., Sackett, P. D., Bridges, T. J., & Freeman, K. C. 2005, *ApJ*, 620, 1043
 Wilson, O. C. 1966, *ApJ*, 144, 695

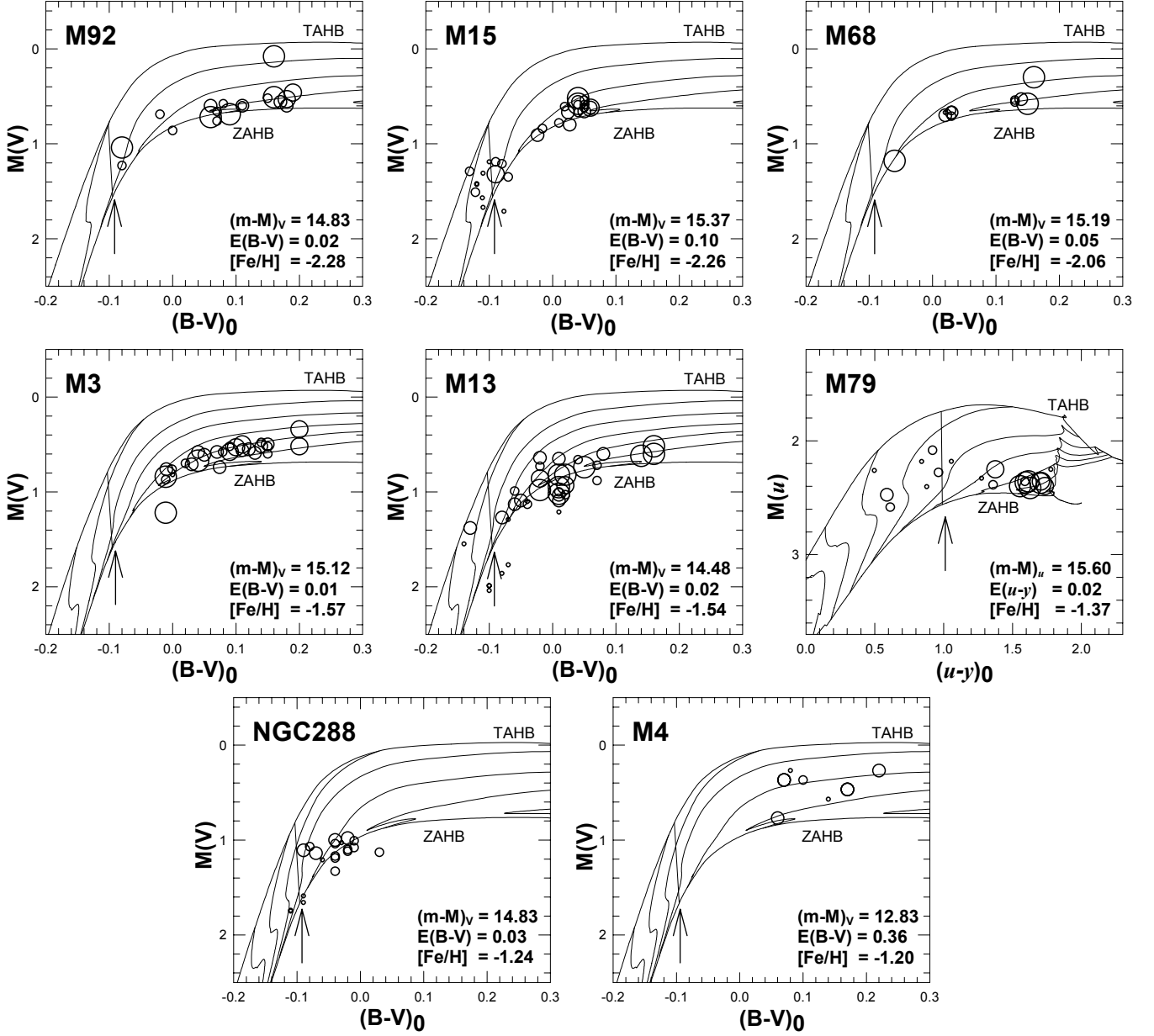


FIG. 10.— Color-magnitude diagram in the Johnson and the Strömgren systems for HB stars in the Galactic GCs M 92, M 15, M 68, M 3, M 13, M 79, NGC 288, and M 4. HB stars with $v \sin i$ measurements are shown as open circles, the sizes of the circles representing different intervals of $v \sin i$ (see Fig. 1). The ZAHB, the TAHB, and evolutionary tracks for several different mass values are also shown (see text). The locus of the Grundahl jump is presented in each panel using a black arrow, and in each panel the points in the evolutionary tracks with $T_{\text{eff}} = 11,500$ K (Grundahl et al. 1999) are connected with a line.

TABLE 3
Physical parameters and Photometry of Field Metal-Poor Stars

Star ID	T_{eff} (K)	$\log(g)$ (cgs)	$v \sin i$ (km s^{-1})	$[Fe/H]$ (dex)	V (mag)	$(B-V)$ (mag)	$(V-I)$ (mag)	Reference
HD20	5350	2.50	5.9	-1.66	9.07	0.54	0.75	3
HD97	5270	2.83	4.0	-1.42	9.40	0.64	0.82	2
...	4910	2.60	4.0	-1.38	9.40	0.64	0.82	3
...	4953	3.10	4.2	-1.40	9.40	0.64	0.82	4
HD2857	7550	3.00	29.0	-1.70	9.95	0.17	0.24	1
...	8002	3.38	25.1	-1.67	9.95	0.17	0.24	2
HD2880	4810	4.01	6.5	-0.83	8.52	0.84	0.88	2
HD3008	4140	1.00	9.2	-1.43	9.70	1.14	1.23	3
...	4140	1.00	4.4	-1.43	9.70	1.14	1.23	5
HD3179	5280	2.60	5.2	-0.92	9.77	0.58	0.78	3
HD4850	8450	3.20	14.0	-1.18	9.64	0.03	...	1
HD5426	4990	2.20	6.3	-2.33	9.63	0.63	0.78	3
...	5114	2.80	5.2	-2.10	9.63	0.63	0.78	4

Continued on Next Page...

TABLE 3 – Continued

Star ID	T_{eff} (K)	$\log(g)$ (cgs)	$v \sin i$ (km s^{-1})	[Fe/H] (dex)	V (mag)	$(B-V)$ (mag)	$(V-I)$ (mag)	Reference
HD6229	5200	1.84	5.7	-1.35	8.60	0.71	0.79	2
HD6268	4800	0.80	7.5	-2.50	8.10	0.79	0.84	4
HD6461	5109	1.86	6.2	-1.30	7.65	0.75	0.82	2
HD6755	5080	2.70	3.5	-1.72	7.73	0.67	0.76	3
HD7374	13327	3.84	20.8	-0.80	5.96	-0.08	-0.06	2
HD8376	8150	3.30	15.0	-2.82	9.59	0.13	...	1
...	7606	2.87	0.0	-3.06	9.59	0.13	...	2
HD9051	4840	2.30	0.5	-1.50	8.92	0.76	0.84	3
HD13359	5150	2.80	8.3	-1.66	9.67	0.69	0.76	3
HD13780	7950	3.10	14.0	-1.53	9.81	0.09	0.11	1
...	7930	3.10	10.0	-1.50	9.81	0.09	0.11	4
HD14829	8900	3.20	7.0	-2.39	10.22	0.08	0.04	1
...	9086	3.31	14.3	-2.01	10.22	0.08	0.04	2
HD16456	7700	2.80	15.0	-1.50	9.04	0.22	0.27	4
HD19445	5911	4.30	10.0	-1.60	8.05	0.46	0.56	4
HD21581	4860	2.30	5.7	-1.65	8.72	0.75	0.82	3
...	4825	2.00	5.0	-1.70	8.72	0.75	0.82	4
HD22879	5808	4.20	4.7	-0.90	6.74	0.49	0.66	4
HD23798	4310	1.00	5.0	-1.90	8.32	1.03	1.01	3
...	4310	1.00	0.0	-1.90	8.32	1.03	1.01	5
...	4566	0.80	6.2	-2.10	4
HD24289	5700	3.50	6.3	-2.20	9.96	0.52	0.60	4
HD24341	5348	3.79	3.5	-0.90	7.86	0.66	0.74	2
HD25532	5553	2.11	7.7	-1.41	8.24	0.61	0.72	2
...	5320	2.54	4.8	-1.33	8.24	0.61	0.72	5
HD25704	5830	4.10	4.8	-1.10	8.10	0.55	0.64	4
HD26297	4500	1.20	5.0	-1.70	7.47	1.08	1.05	4
HD27295	11956	3.92	4.0	-0.95	5.49	-0.07	-0.05	2
HD27928	4990	2.30	1.7	-2.25	9.53	0.69	0.77	3
...	5206	2.90	4.0	-2.00	9.53	0.69	0.77	4
HD29574	4310	0.60	5.5	-1.90	8.38	1.32	1.26	4
...	3960	0.57	3.7	-2.11	8.38	1.32	1.26	5
HD31943	7690	3.20	6.0	-1.00	8.27	0.10	0.14	4
HD34328	5928	4.30	5.5	-1.70	9.46	0.49	0.58	4
HD36702	4180	0.80	6.5	-1.86	8.38	1.15	1.11	3
...	4485	0.80	5.6	-2.00	8.38	1.15	1.11	4
HD44007	4850	2.00	5.0	-1.70	8.06	0.79	0.85	4
HD45282	5230	2.90	5.0	-1.80	8.02	0.65	0.76	3
...	5477	3.30	3.0	-1.40	8.02	0.65	0.76	4
HD46341	5683	4.20	4.0	-0.80	8.60	0.56	0.64	4
HD51754	5830	4.30	3.5	-0.50	9.03	0.57	0.65	4
HD51929	5886	3.50	3.0	-0.50	7.43	0.59	0.66	4
HD56274	5700	4.30	5.0	-0.60	7.79	0.57	0.68	4
HD60778	8050	3.10	13.0	-1.34	9.12	0.07	0.15	1
...	8020	3.13	10.0	-1.48	9.12	0.07	0.15	2
HD63077	5715	4.10	5.0	-1.00	5.37	0.58	0.70	4
HD63598	5852	4.10	4.5	-0.70	7.93	0.54	0.62	4
HD63791	4954	2.17	4.4	-1.72	7.92	0.86	0.89	2
...	4660	1.80	3.7	-1.64	7.92	0.86	0.89	3
HD64488	8826	3.63	150.6	-0.77	7.14	0.16	0.06	2
HD74721	8900	3.30	6.0	-1.48	8.71	0.05	0.06	1
...	8677	3.38	2.6	-1.41	8.71	0.05	0.06	2
...	8900	3.30	1.0	-1.40	8.71	0.05	0.06	4
HD76932	5880	4.00	5.0	-1.00	5.86	0.53	0.59	4
HD78913	8500	3.25	14.0	-1.43	9.29	0.05	0.11	1
...	8515	3.20	10.0	-1.50	9.29	0.05	0.11	4
HD79452	5042	2.14	6.1	-0.91	5.99	0.81	0.86	2
HD82590	6094	2.04	9.7	-1.50	9.42	0.39	0.54	2
...	5960	2.70	7.7	-1.85	9.42	0.39	0.54	5
HD83212	4430	1.40	7.3	-1.45	8.34	1.01	0.99	3
...	4439	1.40	6.0	-1.40	8.34	1.01	0.99	4
HD83220	6546	4.20	8.0	-0.70	8.56	0.35	0.48	4
HD84903	4700	3.30	6.0	-1.40	8.04	1.06	1.03	4
HD84937	6409	3.90	5.2	-2.20	8.28	0.41	0.46	4
HD85773	4450	1.10	7.0	-2.00	9.43	1.08	1.14	4
HD86986	7950	3.20	9.5	-1.66	8.01	0.10	0.13	1
...	7775	3.05	9.2	-1.85	8.01	0.10	0.13	2
...	7950	3.20	13.0	-1.80	8.01	0.10	0.13	4
HD87047	7850	3.10	6.0	-2.43	9.72	0.14	...	1
...	7682	2.95	9.2	-2.36	9.72	0.14	...	2
HD87112	9750	3.50	6.5	-1.56	9.71	-0.02	...	1
...	9557	3.46	7.2	-1.65	9.71	-0.02	...	2
HD93329	8250	3.10	11.0	-1.30	8.76	0.10	0.14	1
...	8042	3.09	9.6	-1.49	8.76	0.10	0.14	2
HD93529	4840	2.40	2.7	-1.24	9.31	0.77	0.83	3

Continued on Next Page...

TABLE 3 – Continued

Star ID	T_{eff} (K)	$\log(g)$ (cgs)	$v \sin i$ (km s^{-1})	[Fe/H] (dex)	V (mag)	$(B-V)$ (mag)	$(V-I)$ (mag)	Reference
...	4840	2.40	8.0	-1.20	9.31	0.77	0.83	4
HD97560	5422	2.39	7.4	-1.06	7.92	0.66	0.72	2
HD97916	6016	4.00	10.2	-1.10	9.17	0.38	0.49	4
HD99383	6143	4.20	4.0	-1.50	9.08	0.48	0.55	4
HD101063	5163	3.40	5.0	-1.10	9.45	0.76	0.80	4
HD103036	4375	0.80	8.0	-1.70	8.18	1.29	1.23	4
HD103376	13554	3.96	189.9	-0.71	10.17	-0.14	-0.11	2
HD103545	4690	1.70	5.0	-2.42	9.20	0.71	0.86	3
...	4725	1.70	5.7	-2.10	9.20	0.71	0.86	4
HD104893	4500	1.10	6.0	-2.20	9.25	1.20	1.18	4
HD105262	8855	1.82	6.1	-1.61	7.09	0.01	0.04	2
HD105546	5299	2.20	5.2	-1.67	8.61	0.79	0.72	2
HD106304	9750	3.50	10.0	-1.34	9.07	0.03	0.04	1
...	9747	3.50	5.0	-1.50	9.07	0.03	0.04	4
HD106373	6160	2.70	10.8	-2.48	8.91	0.40	0.51	5
HD107752	4750	1.70	4.6	-2.64	10.07	0.72	0.84	3
HD108317	5230	2.40	5.1	-2.48	8.03	0.60	0.68	3
HD108577	5192	1.50	5.8	-2.33	9.55	0.63	0.76	2
...	5040	1.90	6.9	-2.50	9.55	0.63	0.76	3
HD109995	8500	3.10	26.0	-1.70	7.60	0.04	0.06	1
...	8382	3.25	22.9	-1.76	7.60	0.04	0.06	2
HD110184	4366	0.50	4.0	-2.40	8.31	1.15	1.11	4
HD110281	3850	0.20	5.5	-1.75	9.39	1.71	1.60	5
HD110679	5001	1.91	5.1	-1.08	9.16	0.86	...	2
HD110885	5330	2.50	8.2	-1.59	9.14	0.60	0.73	3
HD110930	4934	2.31	4.7	-0.94	9.71	0.90	...	2
HD111721	4860	2.50	3.0	-1.42	7.97	0.81	0.83	3
...	4825	2.20	5.0	-1.50	7.97	0.81	0.83	4
HD111777	5693	4.40	5.0	-0.70	8.46	0.61	0.68	4
HD111980	6032	3.70	4.0	-0.70	8.38	0.53	0.62	4
HD112030	4699	1.81	4.3	-1.12	8.70	0.90	...	2
HD113083	5762	4.00	4.5	-0.90	8.05	0.53	0.62	4
HD115444	4736	1.62	4.6	-3.18	9.00	0.70	0.79	2
HD117880	9300	3.30	14.0	-1.51	9.06	0.02	0.09	1
...	7914	2.83	14.5	-2.25	9.06	0.02	0.09	2
...	7880	3.30	16.5	-1.60	9.06	0.02	0.09	4
HD118055	4160	1.00	7.4	-1.46	8.89	1.21	1.23	3
...	4088	0.80	5.0	-1.80	8.89	1.21	1.23	4
HD119516	5689	2.23	8.1	-1.92	9.13	0.39	0.72	2
...	5440	2.50	9.1	-2.49	9.13	0.39	0.72	3
HD121135	4910	1.90	8.6	-1.83	9.30	0.60	0.83	3
HD121261	4210	1.00	8.0	-1.52	9.21	1.29	1.20	3
...	4210	1.00	5.0	-1.50	9.21	1.29	1.20	4
HD122563	4697	1.30	5.0	-2.60	6.20	0.90	0.87	4
HD122956	4530	1.60	6.3	-1.71	7.25	0.93	0.93	3
...	4575	1.10	8.0	-1.80	7.25	0.93	0.93	4
HD124358	4640	1.50	6.7	-1.98	9.54	0.84	0.96	3
HD126238	4979	2.50	5.0	-1.70	7.68	0.76	0.82	4
HD126587	4850	1.80	4.3	-2.58	9.15	0.73	0.81	3
HD128279	5275	2.80	5.0	-2.00	7.97	0.63	0.70	4
HD128801	10300	3.55	9.0	-1.56	8.73	-0.04	-0.02	1
...	10162	3.54	8.6	-1.38	8.73	-0.04	-0.02	2
HD130095	9000	3.30	9.5	-2.04	8.13	0.07	0.05	1
...	9000	3.30	7.0	-1.80	8.13	0.07	0.05	4
HD130201	8650	3.50	16.0	-0.86	10.07	0.08	...	1
HD132475	5920	3.60	5.0	-1.10	8.57	0.53	0.58	4
HD134169	5861	3.90	5.2	-0.80	7.67	0.49	0.64	4
HD135148	4180	0.80	7.8	-1.88	9.40	1.21	1.36	3
HD136316	4998	1.10	4.0	-1.40	7.65	1.12	1.08	4
HD139961	8500	3.20	37.0	-1.68	8.86	0.08	0.11	1
HD140283	5928	3.40	5.0	-2.00	7.24	0.45	0.56	4
HD141531	4340	1.10	7.5	-1.57	9.15	1.15	1.20	3
HD143459	9990	3.57	36.8	-0.84	5.53	0.04	0.06	2
HD145293	6394	3.04	9.8	-1.11	10.03	0.58	0.73	2
HD145417	4953	4.50	5.0	-1.20	7.52	0.82	0.94	4
HD145598	5525	4.40	5.0	-0.60	8.66	0.66	0.72	4
HD148704	5096	4.00	6.2	-0.50	7.24	0.86	0.90	4
HD148816	5882	4.00	5.7	-0.70	7.27	0.54	0.65	4
HD149414	5437	4.40	5.0	-1.00	9.63	0.74	0.90	4
HD149996	5700	3.90	5.0	-0.60	8.49	0.61	0.68	4
HD158809	5450	3.80	5.0	-0.50	8.13	0.64	0.72	4
HD159482	5987	4.30	5.0	-1.00	8.39	0.56	0.69	4
HD160617	6209	3.80	6.2	-1.70	8.73	0.45	0.53	4
HD161770	5696	3.69	2.6	-1.81	9.66	0.66	0.73	2
...	5547	3.90	5.8	-2.00	9.66	0.66	0.73	4

Continued on Next Page...

TABLE 3 – Continued

Star ID	T_{eff} (K)	$\log(g)$ (cgs)	$v \sin i$ (km s^{-1})	[Fe/H] (dex)	V (mag)	$(B-V)$ (mag)	$(V-I)$ (mag)	Reference
HD161817	7550	3.00	17.0	-1.64	6.99	0.14	0.27	1
...	7711	3.22	15.2	-1.52	6.99	0.14	0.27	2
HD163799	5859	3.90	5.2	-0.90	8.81	0.54	0.62	4
HD163810	5523	4.10	6.0	-1.10	9.62	0.62	0.68	4
HD165195	4200	0.76	1.8	-2.16	7.34	1.24	1.19	5
...	4100	0.80	5.0	-1.90	7.34	1.24	1.19	4
HD167105	9050	3.30	21.5	-1.66	8.93	0.04	0.04	1
...	8875	3.37	20.0	-1.62	8.93	0.04	0.04	2
HD167768	4823	0.82	6.8	-1.54	6.00	0.89	0.99	2
HD171496	4820	2.30	7.1	-1.16	8.52	1.07	1.04	3
...	4700	1.60	7.0	-0.90	8.52	1.07	1.04	4
HD175179	5830	3.90	4.4	-0.70	9.04	0.58	0.66	4
HD175305	5149	3.23	3.5	-1.39	7.20	0.73	0.89	2
HD176203	4820	2.40	6.8	-1.81	8.79	0.69	0.78	3
HD179626	6106	3.70	4.0	-0.80	9.14	0.53	0.61	4
HD180903	7700	3.10	18.5	-1.32	9.61	0.15	...	1
HD181007	4770	2.00	4.2	-2.00	9.63	0.78	0.83	3
HD184266	5760	1.82	9.3	-1.73	7.57	0.59	0.62	2
...	5500	2.50	8.5	-1.50	7.57	0.59	0.62	4
...	5490	2.60	5.0	-1.87	7.57	0.59	0.62	5
HD186478	4540	1.40	5.3	-2.45	9.18	0.90	0.96	3
HD187111	4260	1.04	2.4	-1.65	7.75	1.17	1.13	5
HD189558	5602	3.70	5.2	-1.10	7.72	0.55	0.64	4
HD192031	5324	4.40	5.0	-0.80	8.66	0.72	0.78	4
HD195019	4727	1.80	4.3	-2.32	6.91	0.64	0.72	2
HD195636	5399	1.93	20.6	-2.74	9.57	0.56	0.71	2
...	5370	2.40	22.2	-2.40	9.57	0.56	0.71	5
HD199288	5655	4.20	5.0	-0.60	6.52	0.59	0.68	4
HD199289	5984	4.30	4.0	-0.80	8.30	0.52	0.61	4
HD199854	6338	2.18	24.3	-1.71	8.97	0.35	0.46	2
HD200654	5477	3.60	4.0	-2.40	9.11	0.63	0.65	4
HD200973	6453	3.90	4.8	-0.50	7.22	0.46	0.53	4
HD201099	5912	4.00	5.3	-0.50	7.60	0.52	0.62	4
HD202759	7500	3.05	11.0	-2.35	9.11	0.17	0.22	1
HD203854	5923	0.84	198.9	-2.26	9.15	0.48	...	2
HD204543	5365	1.20	4.0	-2.00	8.60	0.76	0.89	4
HD206739	4620	1.80	5.1	-1.57	8.70	0.89	0.98	3
...	4930	1.70	5.3	-1.60	8.70	0.89	0.98	4
HD208069	5030	2.60	3.7	-1.83	9.25	0.68	0.75	3
HD208110	5101	2.11	4.8	-1.26	6.16	0.75	0.82	2
HD212038	5076	4.50	4.4	-0.50	8.79	0.79	0.88	4
HD213467	5010	2.80	1.5	-1.45	8.58	0.68	0.74	3
HD213468	9150	3.30	12.0	-1.67	10.78	0.10	...	1
HD214362	5700	2.60	7.5	-2.20	9.10	0.46	0.58	5
HD214925	3890	0.30	4.5	-2.14	9.30	1.47	1.50	5
HD215257	5978	4.40	3.0	-0.70	7.46	0.47	0.59	4
HD217515	6727	3.79	9.7	-1.02	9.36	0.36	0.42	2
HD218732	3900	0.20	11.1	-2.00	8.47	1.52	1.56	3
HD218732	3900	0.20	3.1	-2.00	8.47	1.52	1.56	5
HD219617	5825	4.30	6.2	-1.50	8.16	0.47	0.62	4
HD220662	4450	1.30	3.0	-1.75	10.03	1.09	1.01	3
HD220787	17747	3.75	26.3	-0.55	8.29	-0.15	-0.19	2
HD220838	4280	1.10	6.5	-1.53	9.39	1.11	1.12	3
HD221170	4410	1.10	1.0	-1.56	7.71	1.02	1.00	5
HD222434	4430	1.30	5.0	-1.56	8.81	1.04	1.04	3
...	4477	1.10	5.4	-1.70	8.81	1.04	1.04	4
HD229274	5690	2.46	6.7	-1.40	9.06	0.57	0.69	2
HD233666	5874	3.15	5.3	-1.31	9.34	0.60	0.71	2
HD252940	7550	2.95	24.5	-1.80	9.10	0.30	0.31	1
...	7652	3.11	22.9	-1.70	9.10	0.30	0.31	2
HD274939	5282	3.00	3.0	-1.20	9.45	0.68	0.79	4
BD+00 0145	9121	4.18	27.8	-2.47	10.60	0.14	...	2
BD+01 0514	7673	3.10	137.9	-2.00	9.69	0.21	...	2
BD+01 0548	8714	3.38	10.2	-2.23	10.79	-0.05	...	2
BD+03 0740	6406	3.76	6.0	-2.87	9.82	0.36	0.48	2
BD+09 3223	5305	1.91	5.4	-2.34	9.25	0.56	0.69	2
BD+1 3070	5130	2.70	5.0	-1.85	9.99	0.63	0.81	3
BD+3 2782	4500	1.30	5.3	-2.01	9.72	0.90	1.05	3
BD+3 740	6075	3.80	1.5	-2.80	9.82	0.36	0.48	4
BD+5 3098	4930	2.00	5.2	-2.40	10.40	0.80	0.82	3
BD+6 648	4500	1.10	6.0	-2.10	9.09	1.18	1.24	4
...	4160	0.87	1.2	-1.82	9.09	1.18	1.24	5
BD+8 2856	4480	1.10	8.9	-2.31	9.96	0.89	0.96	3
...	4480	1.10	7.0	-2.30	9.96	0.89	0.96	4
BD+9 2574	4860	2.10	2.5	-1.95	10.34	0.74	0.82	3

Continued on Next Page...

TABLE 3 – Continued

Star ID	T_{eff} (K)	$\log(g)$ (cgs)	$v \sin i$ (km s^{-1})	[Fe/H] (dex)	V (mag)	$(B-V)$ (mag)	$(V-I)$ (mag)	Reference
BD+9 2860	5240	2.50	3.9	-1.67	10.74	0.53	0.76	3
BD+9 2870	4600	1.40	5.2	-2.37	9.70	0.88	1.01	3
BD+9 3223	5310	2.40	4.8	-2.41	9.25	0.56	0.69	3
BD+10 2495	5275	2.75	2.6	-2.07	9.69	0.63	0.79	2
...	4920	2.20	3.8	-2.14	9.69	0.63	0.79	3
...	5027	1.40	3.0	-2.00	9.69	0.63	0.79	4
BD+11 2998	5647	2.39	6.6	-1.28	9.07	0.63	0.73	2
...	5360	2.50	6.8	-1.46	9.07	0.63	0.73	3
BD+12 2547	4610	1.50	3.9	-2.07	9.92	0.83	1.01	3
BD+13 3683	5540	3.10	5.1	-1.90	10.55	0.64	0.73	3
BD+14 4757	6390	4.99	2.1	-0.56	10.14	0.43	...	2
BD+17 3248	5398	2.21	5.4	-2.08	9.37	0.62	0.73	2
BD+17 4708	6297	4.40	3.5	-1.61	9.45	0.43	0.53	2
BD+18 2757	4741	1.16	5.5	-2.43	9.83	0.77	0.81	2
...	4840	1.70	7.8	-2.52	9.83	0.77	0.81	3
BD+18 2890	5347	2.60	3.2	-1.78	9.77	0.72	0.84	2
...	4970	2.50	5.1	-1.61	9.77	0.72	0.84	3
BD+18 2976	4550	1.30	5.2	-2.42	9.85	0.78	1.02	3
BD+20 3004	14549	3.80	104.7	-0.91	10.04	-0.06	-0.12	2
BD+22 2411	4320	1.00	0.0	-1.95	9.95	1.25	1.21	5
BD+25 1981	7302	4.41	7.9	-1.43	9.29	0.36	0.36	2
BD+25 2436	4847	2.14	6.1	-0.76	9.92	0.89	...	2
BD+25 2497	5169	2.42	5.1	-0.84	10.29	0.91	...	2
BD+25 2602	8400	3.20	16.0	-1.98	10.14	0.04	0.07	1
...	8250	3.26	13.3	-2.08	10.14	0.04	0.07	2
BD+27 2057	4695	1.58	6.5	-1.25	9.44	0.99	...	2
BD+29 2231	4756	2.39	4.8	-0.65	9.81	0.92	...	2
BD+29 2294	5132	3.18	5.0	-0.55	9.51	0.82	...	2
BD+30 2355	10215	3.29	97.3	-2.70	10.65	-0.10	-0.04	2
BD+30 2034	4290	1.00	8.9	-1.53	10.40	1.40	1.23	3
BD+32 2188	10450	2.10	2.5	-1.45	10.65	0.01	-0.01	1
...	10257	2.00	0.4	-1.05	10.65	0.01	-0.01	2
BD+33 2171	7149	3.72	44.0	-1.73	10.63	0.15	0.33	2
BD+36 2242	11650	4.01	77.1	-0.84	9.91	-0.06	-0.04	2
BD+36 2303	4705	2.40	5.1	-0.77	9.54	1.02	...	2
BD+42 2309	8800	3.20	35.0	-1.62	10.82	-0.02	0.06	1
...	8796	3.39	30.7	-1.69	10.82	-0.02	0.06	2
BD+44 493	5510	2.60	3.9	-2.71	9.13	0.46	0.78	3
BD-02 0524	16563	3.75	11.9	-0.63	10.34	-0.13	-0.11	2
BD-1 1792	4850	2.70	4.6	-1.20	9.25	0.82	0.84	4
BD-1 2582	5130	2.40	6.9	-2.32	9.60	0.67	0.78	3
...	5130	2.40	10.0	-2.30	9.60	0.67	0.78	4
BD-3 5215	5420	2.60	7.3	-1.64	10.13	0.68	0.77	3
BD-8 3901	4600	1.90	4.3	-1.88	9.44	0.90	0.91	3
BD-9 5831	4550	1.40	5.1	-1.87	9.50	0.83	0.96	3
...	5327	1.40	3.0	-2.00	9.50	0.83	0.96	4
BD-10 548	4900	2.40	3.0	-1.71	10.60	0.44	0.81	3
...	5706	3.00	4.0	-1.50	10.60	0.44	0.81	4
BD-11 145	4780	1.70	5.2	-2.02	10.60	0.70	0.91	3
BD-12 2669	6880	3.91	32.0	-2.04	10.22	0.33	0.36	2
BD-14 5890	4840	2.10	2.2	-2.01	10.31	0.78	0.90	3
BD-15 5781	4590	1.60	3.4	-2.47	10.80	0.70	0.97	3
BD-17 6036	4830	1.90	3.9	-2.54	10.60	0.60	0.86	3
BD-18 271	4150	0.70	0.0	-1.98	9.85	1.06	1.18	5
BD-18 5550	4820	1.80	3.9	-3.11	9.35	0.68	0.76	3
BD-19 1422	4800	2.20	5.6	-1.86	9.77	0.73	0.82	3
BD-20 170	5130	2.50	5.4	-1.31	10.31	0.60	0.80	3
BD-20 6008	4550	1.30	0.5	-2.63	9.89	0.71	0.87	3
BD-22 395	4780	1.70	6.5	-2.14	10.60	0.70	0.83	3
BPSCS22189-5	7397	3.60	13.9	-1.00	14.18	0.31	...	2
BPSCS22894-36	7832	4.12	10.2	-1.77	14.76	0.28	...	2
CD-23 72	5270	2.50	8.9	-1.12	9.20	0.58	0.76	3
CD-24 1782	5300	2.80	8.0	-2.80	9.97	0.57	0.71	4
CD-30 1121	4940	2.40	2.5	-1.82	10.33	0.67	0.81	3
CD-30 298	5120	2.40	3.5	-2.90	10.70	0.60	0.73	3
CD-30 8626	5000	2.20	5.0	-1.67	9.70	0.73	0.82	3
CD-33 9314	4820	2.00	5.0	-2.10	10.04	0.64	0.82	3
CD-36 1052	5890	2.50	8.8	-2.00	10.00	0.37	0.54	5
CD-37 14010	4300	0.90	19.4	-2.55	9.74	1.01	0.97	3
CD-38 245	4920	1.80	3.4	-4.00	12.00	0.73	0.84	3
Feige40	15904	4.54	120.7	-1.71	11.10	0.00	-0.13	2
Feige84	18587	4.45	111.0	< -1.54	11.40	0.10	-0.17	2
GCRV63536	8702	4.29	10.9	-0.83	11.17	0.16	...	2
HZ27	9883	3.38	6.6	-1.39	10.43	2
PG0855+294	20049	5.64	135.5	< -1.74	2

Continued on Next Page...

TABLE 3 – Continued

Star ID	T_{eff} (K)	$\log(g)$ (cgs)	$v \sin i$ (km s^{-1})	[Fe/H] (dex)	V (mag)	$(B-V)$ (mag)	$(V-I)$ (mag)	Reference
PG1205+228	16271	3.06	175.1	< -2.27	11.01	-0.13	-0.17	2
PG2219+094	17402	3.91	225.3	-1.88	2
PHL3275	4734	2.81	2.8	-0.73	11.20	0.90	...	2

REFERENCES:

- (1) Kinman et al. 2000.
- (2) Behr 2003a.
- (3) Carney et al. 2003.
- (4) De Medeiros et al. 2006.
- (5) Carney et al. 2008.

TABLE 4
Physical parameters and Photometry of Metal-Poor Stars in Globular Cluster

Star ID	T_{eff} (K)	$\log(g)$ (cgs)	$v \sin i$ (km s^{-1})	[Fe/H] (dex)	V (mag)	$(B-V)$ (mag)	OTHER (mag)	M_V (mag)	$(B-V)_0$ (mag)	Reference
M3/19	7607	3.01	7.40	...	15.64	0.16	...	0.52	0.15	2
M3/20	7640	3.02	10.60	...	15.64	0.15	...	0.52	0.14	2
M3/54	7764	3.05	11.80	...	15.67	0.13	...	0.55	0.12	2
M3/97	7579	3.01	14.80	...	15.62	0.16	...	0.50	0.15	2
M3/109	7583	3.01	9.20	...	15.60	0.15	...	0.48	0.14	2
M3/168,1371,AX	7702	3.04	16.00	...	15.62	0.12	...	0.50	0.11	2
M3/201,1130,II-63	7818	3.07	12.70	...	15.68	0.12	...	0.56	0.11	2
M3/237	7932	3.09	18.60	...	15.70	0.10	...	0.58	0.09	2
M3/378,258,Z	8078	3.13	12.20	...	15.70	0.05	...	0.58	0.04	2
M3/444,343,III-72	7331	2.94	15.70	...	15.46	0.21	...	0.34	0.20	2
M3/512	9166	3.37	1.60	...	15.94	0.01	...	0.82	0.00	2
M3/518	7996	3.11	11.70	...	15.70	0.08	...	0.58	0.07	2
...	8224	3.21	5.87	-1.63	15.70	0.08	...	0.58	0.07	5
M3/523,1335,I-51	7822	3.07	13.90	...	15.71	0.14	...	0.59	0.13	2
M3/701	7797	3.06	9.80	...	15.64	0.10	...	0.52	0.09	2
M3/760	7430	2.97	15.50	...	15.64	0.21	...	0.52	0.20	2
M3/831	8890	3.22	13.50	...	15.88	0.00	...	0.76	-0.01	2,6
...	9148	3.41	9.99	-1.52	15.88	0.00	...	0.76	-0.01	5
M3/885	8572	3.26	9.90	...	15.82	0.03	...	0.70	0.02	2,6
M3/1038	7784	3.06	16.30	...	15.65	0.11	...	0.53	0.10	2
M3/1060	8138	3.14	11.20	...	15.73	0.06	...	0.61	0.05	2
M3/1195,1009	8600	3.34	10.70	...	15.83	0.04	...	0.71	0.03	2,6
M3/1228	8391	3.36	20.70	...	15.79	0.05	...	0.67	0.04	2,6
M3/1280	9801	3.49	8.70	...	15.72	0.16	...	0.60	0.15	2
M3/B1241	9600	3.50	6.48	-1.38	15.99	-0.01	...	0.87	-0.02	5
M3/B125	8937	3.43	14.72	-1.51	15.86	0.08	0.05 ^{aa}	0.74	0.07	5
M3/B244	9408	3.48	33.70	-1.44	15.96	-0.01	-0.06 ^a	0.84	-0.02	5
M3/B445	10047	3.71	31.97	-2.25	16.34	-0.01	-0.01 ^a	1.22	-0.02	5
M4/2602	14.00	...	13.30	0.53	...	0.47	0.17	1
M4/2613	11.00	...	13.60	0.42	...	0.77	0.06	1
M4/2614	3.00	...	13.40	0.50	...	0.57	0.14	1
M4/2616	13.00	...	13.10	0.58	...	0.27	0.22	1
M4/3301	7.00	...	13.20	0.46	...	0.37	0.10	1
M4/3307	11.00	...	13.20	0.43	...	0.37	0.07	1
M4/3315	14.00	...	13.20	0.43	...	0.37	0.07	1
M4/3511	3.00	...	13.10	0.44	...	0.27	0.08	1
M4/3633	10.00	...	13.30	0.53	...	0.47	0.17	1
M13/I-3	10335	3.65	9.30	...	15.48	0.03	...	1.00	0.01	2
M13/I-8	12749	4.09	13.60	...	15.86	-0.11	...	1.38	-0.13	2
M13/I-15	9629	3.50	7.80	...	15.36	0.09	...	0.88	0.07	2
M13/I-21	8981	3.35	7.80	...	15.21	0.00	...	0.73	-0.02	2
M13/I-57	9385	3.45	32.70	...	15.30	0.03	...	0.82	0.01	2
M13/I-64	7970	3.10	29.80	...	15.08	0.18	...	0.60	0.16	2
M13/I-89	8151	3.15	26.30	...	15.10	0.16	...	0.62	0.14	2
M13/II-5	10502	3.68	13.40	...	15.51	0.03	...	1.03	0.01	2
M13/II-19	10845	3.75	10.60	...	15.57	0.03	...	1.09	0.01	2
M13/II-22	10446	3.67	20.00	...	15.50	0.03	...	1.02	0.01	2
M13/II-61	10886	3.76	13.90	...	15.57	-0.03	...	1.09	-0.05	2
M13/II-65	10496	3.68	8.60	...	15.51	0.04	...	1.03	0.02	2
M13/II-68	8595	3.26	10.10	...	15.13	0.03	...	0.65	0.01	2
M13/II-83	8600	3.26	13.00	...	15.12	0.00	...	0.64	-0.02	2
M13/III-38	11127	3.80	14.40	...	15.61	-0.04	...	1.13	-0.06	2
M13/III-58	8829	3.32	9.90	...	15.20	0.09	...	0.72	0.07	2
M13/III-70	10056	3.59	23.60	...	15.43	0.03	...	0.95	0.01	2
M13/IV-23	12000	3.96	11.30	...	15.75	-0.06	...	1.27	-0.08	2
M13/IV-81	10246	3.63	37.60	...	15.46	0.00	...	0.98	-0.02	2
M13/IV-83	8450	3.28	32.85	-1.81	15.22	0.06	...	0.74	3.26	5
M13/J11	7681	3.08	22.23	-1.81	15.00	0.17	...	0.52	3.06	5
M13/J24	9375	3.44	39.30	...	15.30	0.04	...	0.82	0.02	2
M13/J431	9944	3.57	19.10	...	15.41	0.04	...	0.93	0.02	2
M13/J52	8244	3.17	14.00	...	15.08	0.10	...	0.60	0.08	2
M13/J7	10329	3.65	9.70	...	15.47	-0.04	...	0.99	-0.06	2
M13/SA113	10363	3.72	4.88	-1.73	15.69	0.02	...	1.21	3.70	5
M13/SA368	8586	3.26	8.90	...	15.14	0.06	...	0.66	0.04	2
M13/SA404	10449	3.66	2.33	-1.74	15.58	-0.03	...	1.10	3.64	5
M13/SA581	11115	3.80	5.80	...	15.61	-0.02	...	1.13	-0.04	2
M13/WF2-820	11838	3.90	6.32	-0.22	16.84	-0.07	...	2.36	3.88	5
M13/WF2-2541	13353	4.18	4.17	-0.27	16.03	-0.13	-0.06 ^a	1.55	4.16	5
M13/WF2-2692	12530	4.08	0.00	-0.23	16.47	-0.09	-0.11 ^a	1.99	4.06	5
M13/WF2-3035	9367	3.47	4.64	-1.53	16.34	-0.07	...	1.86	3.45	5
M13/WF2-3123	13667	4.31	16.01	-0.71	15.34	-0.01	0.05 ^a	0.86	4.29	5
M13/WF3-548	13103	4.16	1.89	-0.64	15.77	-0.06	...	1.29	4.14	5
M13/WF3-1718	11513	3.79	4.29	0.02	16.52	-0.09	...	2.04	3.77	5
M13/WF4-3085	14200	4.15	3.63	0.7	16.23	1.75	...	5

Continued on Next Page...

TABLE 4 – Continued

Star ID	T_{eff} (K)	$\log(g)$ (cgs)	$v \sin i$ (km s^{-1})	[Fe/H] (dex)	V (mag)	($B-V$) (mag)	OTHER (mag)	M_V (mag)	($B-V$) ₀ (mag)	Reference
M13/WF4-3485	13151	4.08	3.23	-0.08	16.25	-0.06	...	1.77	4.06	5
M15/699	10839	3.88	23.00	...	16.63	...	0.06 ^a	1.26	...	4
M15/768	12190	4.01	4.00	...	16.94	-0.01	...	1.57	-0.11	4
M15/788	8017	3.52	7.00	...	15.94	...	0.24 ^a	0.57	...	4
M15/817	11967	3.99	4.00	...	17.04	-0.01	...	1.67	-0.11	4
M15/1048	11429	3.94	11.00	...	16.79	...	0.03 ^a	1.42	...	4
M15/1813	8511	3.59	10.00	...	16.04	0.12	...	0.67	0.02	4
M15/2700	13521	4.14	7.00	...	16.66	-0.03	...	1.29	-0.13	4
M15/2917	8433	3.58	7.00	...	15.98	0.12	...	0.61	0.02	4
M15/3333	8570	3.60	12.00	...	16.17	0.13	...	0.80	0.03	4
M15/4047	8610	3.60	5.00	...	16.15	0.11	...	0.78	0.01	4
M15/4536	10544	3.84	4.00	...	17.08	0.02	...	1.71	-0.08	4
M15/5168	12823	4.07	6.00	...	16.88	-0.02	...	1.51	-0.12	4
M15/5516	8954	3.65	12.00	...	16.28	0.08	...	0.91	-0.02	4
M15/6143	8995	3.65	5.00	...	16.21	0.08	...	0.84	-0.02	4
M15/B78	8198	3.15	9.35	-2.36	15.99	0.15	0.30 ^a	0.62	0.05	5
M15/B84	12013	3.68	4.89	-0.12	16.56	0.00	0.03 ^a	1.19	-0.10	5
M15/B124	8085	3.10	5.60	-2.31	15.91	0.15	0.33 ^a	0.54	0.05	5
M15/B130	8995	3.65	5.00	...	15.96	0.15	...	0.59	0.05	4
M15/B130	8465	3.19	3.40	-2.44	15.96	0.15	0.26 ^a	0.59	0.05	5
M15/B153	8368	3.17	30.13	-2.45	15.95	0.14	...	0.58	0.04	5
M15/B177	8206	3.17	10.60	-2.25	16.03	0.15	...	0.66	0.05	5
M15/B203	13993	3.84	4.89	0.02	16.68	-0.01	-0.02 ^a	1.31	-0.11	5
M15/B218	8091	3.53	13.00	...	15.99	0.16	...	0.62	0.06	4
...	8302	3.18	16.09	-2.46	15.99	0.16	0.28 ^a	0.62	0.06	5
M15/B244	8342	3.16	9.47	-2.4	15.96	0.14	...	0.59	0.04	5
M15/B267	11196	3.69	6.67	0.08	16.72	0.03	...	1.35	-0.07	5
M15/B279	11270	3.63	5.92	0.25	16.56	0.01	...	1.19	-0.09	5
M15/B315	12892	3.81	1.72	0.04	16.80	-0.02	...	1.43	-0.12	5
M15/B331	8445	3.20	8.03	-2.3	16.04	0.14	...	0.67	0.04	5
M15/B334	10748	3.61	9.22	-2.37	16.58	0.02	0.12 ^a	1.21	-0.08	5,7
M15/B348	12150	4.20	17.54	-2.26	16.69	0.01	0.06 ^a	1.32	-0.09	5
M15/B374	12820	3.82	3.92	0.24	16.79	-0.02	...	1.42	-0.12	5
M15/B424	8563	3.18	38.26	-2.36	15.89	0.14	0.25 ^a	0.52	0.04	5
M15/B558	8250	3.14	10.23	-2.51	15.93	0.14	0.30 ^a	0.56	0.04	5
M68/W71	8957	3.37	10.65	-2.19	15.89	0.07	0.13 ^a	0.70	0.02	5
M68/W72	10914	3.70	21.98	-2.27	16.37	-0.01	0.02 ^a	1.18	-0.06	5
M68/W114	7861	3.13	7.60	-2.36	15.73	0.18	0.26 ^a	0.54	0.13	5
M68/W120	8698	3.32	11.16	-2.34	15.86	0.08	0.10 ^a	0.67	0.03	5
M68/W161	8754	3.35	6.09	-2.24	15.90	0.08	0.14 ^a	0.71	0.03	5
M68/W279	8964	3.37	4.81	-2.34	15.86	0.07	0.12 ^a	0.67	0.02	5
M68/W324	7758	3.13	34.08	-2.28	15.77	0.20	0.29 ^a	0.58	0.15	5
M68/W340	7876	3.15	7.52	-2.36	15.75	0.18	0.26 ^a	0.56	0.13	5
M68/W464	7532	2.96	30.62	-2.25	15.49	0.21	0.35 ^a	0.30	0.16	5
M68/W468	8890	3.35	5.64	-2.17	15.84	0.08	0.12 ^a	0.65	0.03	5
M68/W510	7630	3.07	13.88	-2.33	15.72	0.19	0.34 ^a	0.53	0.14	5
M79/209	7430	2.96	3.00	-1.48	17.85; 1.78 ^b	0.47	...	4,8
M79/243	7727	3.04	16.00	17.96; 1.72 ^b	0.64	...	4
M79/275	7745	3.04	27.00	17.97; 1.72 ^b	0.66	...	4
M79/281	8241	3.17	5.00	-1.37	17.96; 1.61 ^b	0.76	...	4,8
M79/289	8128	3.15	22.00	17.96; 1.64 ^b	0.73	...	4
M79/294	7603	3.01	20.00	17.99; 1.75 ^b	0.65	...	4
M79/295	8054	3.13	26.00	18.02; 1.65 ^b	0.78	...	4
M79/297	9268	3.42	20.00	17.85; 1.39 ^b	0.87	...	4
M79/298	8204	3.16	26.00	17.97; 1.62 ^b	0.76	...	4
M79/327	8395	3.21	24.00	18.00; 1.57 ^b	0.84	...	4
M79/354	9795	3.54	5.00	-1.17	17.93; 1.29 ^b	1.05	...	4,8
M79/363	11614	3.89	10.00	0.49	17.87; 0.98 ^b	1.31	...	4
M79/366	9354	3.44	7.00	17.99; 1.38 ^b	1.02	...	4
M79/389	11041	3.79	5.00	0.39	17.78; 1.08 ^b	1.12	...	4,8
M79/392	11912	3.95	6.00	0.42	17.68; 0.94 ^b	1.16	...	4,8
M79/434	12445	4.04	3.00	0.39	17.78; 0.86 ^b	1.33	...	4,8
M79/469	12190	4.00	3.00	0.60	18.00; 0.90 ^b	1.52	...	4,8
M79/489	15276	4.47	5.00	0.36	17.86; 0.52 ^b	1.76	...	4,8
M79/535	14388	4.34	13.00	0.39	18.08; 0.61 ^b	1.88	...	4,8
M79/555	14158	4.31	8.00	18.18; 0.63 ^b	1.96	...	4
M80/83	9727	3.52	10.00	...	16.57	...	0.27 ^a	1.01	...	4
M80/107	11194	3.82	6.00	...	16.88	...	0.22 ^a	1.32	...	4
M80/109	10814	3.74	3.00	...	16.86	...	0.23 ^a	1.30	...	4
M80/454	23442	5.37	4.00	...	18.70	...	0.03 ^a	3.14	...	4
M80/509	8831	3.32	7.00	16.62; 0.22 ^c	4
M80/820	8974	3.35	8.00	16.68; 0.21 ^c	4
M80/1149	17742	4.78	9.00	...	18.15	...	0.10 ^a	2.59	...	4

Continued on Next Page...

TABLE 4 – Continued

Star ID	T_{eff} (K)	$\log(g)$ (cgs)	$v \sin i$ (km s^{-1})	[Fe/H] (dex)	V (mag)	($B-V$) (mag)	OTHER (mag)	M_V (mag)	($B-V$) ₀ (mag)	Reference
M80/1400	11143	3.81	5.00	18.14;0.14 ^c	4
M80/2044	11298	3.84	8.00	16.99;0.14 ^c	4
M80/2242	24266	5.44	7.00	18.74;0.01 ^c	4
M80/938	12560	4.06	5.00	16.89;-0.15 ^c	4
M92/IV-17	9375	3.60	15.00	...	15.50	0.02	0.01 ^d	0.86	0.00	3
...	9419	3.47	8.93	-2.45	15.50	0.02	...	0.86	0.00	5
M92/IV-27	7550	3.10	27.00	...	15.19	0.17	0.12 ^d	0.55	0.15	3
...	7601	3.11	15.93	-2.34	15.19	0.17	...	0.55	0.15	5
M92/VI-10	7763	3.16	6.49	-2.58	15.24	0.13	...	0.60	0.11	5
M92/X-22	7450	3.10	15.00	...	15.16	0.17	0.08 ^d	0.52	0.15	3
...	7495	3.07	8.00	-2.69	15.16	0.17	...	0.52	0.15	5
M92/XII-1	7325	3.00	43.00	...	15.11	0.19	0.07 ^d	0.47	0.17	3
...	7303	3.01	26.69	-2.45	15.11	0.19	...	0.47	0.17	5
M92/XII-9	7500	3.10	29.00	...	15.09	0.15	0.09 ^d	0.45	0.13	3
...	7479	3.03	16.45	-2.38	15.09	0.15	...	0.45	0.13	5
M92/B29	8457	3.35	14.85	-2.40	15.24	0.13	0.12 ^a	0.60	0.11	5
M92/B30	7420	3.06	15.78	-2.39	15.17	0.20	...	0.53	0.18	5
M92/B103	7365	3.08	14.14	-2.55	15.24	0.20	...	0.60	0.18	5
M92/B145	9118	3.12	21.04	-2.19	14.72	0.18	0.07 ^a	0.08	0.16	5
M92/B148	8090	3.26	36.93	-2.39	15.33	0.11	...	0.69	0.09	5
M92/B176	11146	3.76	6.96	-2.25	15.87	-0.06	-0.02 ^a	1.23	-0.08	5
M92/B202	7643	3.13	19.82	-2.24	15.10	0.21	0.27 ^a	0.46	0.19	5
M92/B219	7828	3.18	34.23	-2.35	15.15	0.18	0.23 ^a	0.51	0.16	5
M92/B233	8330	3.33	28.43	-2.20	15.36	0.08	...	0.72	0.06	5
M92/B246	7424	3.06	11.22	-2.54	15.20	0.19	...	0.56	0.17	5
M92/B251	8338	3.28	9.37	-2.52	15.22	0.10	0.16 ^a	0.58	0.08	5
M92/B365	11510	3.71	38.96	-2.20	15.68	-0.06	...	1.04	-0.08	5
M92/B455	8333	3.29	14.94	-2.44	15.24	0.08	...	0.60	0.06	5
M92/B466	8174	3.27	9.11	-2.42	15.30	0.09	...	0.66	0.07	5
M92/B516	8238	3.32	5.39	-2.47	15.40	0.09	...	0.76	0.07	5
M92/B527	9397	3.40	7.79	-2.14	15.33	0.00	...	0.69	-0.02	5
NGC288/10	9745	3.42	11.90	...	15.97	-0.04	...	1.14	-0.07	2,6
NGC288/23	9031	3.10	10.20	...	15.81	0.01	...	0.98	-0.02	2,6
NGC288/28	10617	3.70	5.40	...	16.16	-0.01	...	1.33	-0.04	2,6
NGC288/52	9957	3.46	7.40	...	16.02	-0.01	...	1.19	-0.04	2,6
NGC288/177	9295	3.18	5.50	...	15.87	-0.01	...	1.04	-0.04	2,6
NGC288/200	9152	3.11	9.20	...	15.84	0.02	...	1.01	-0.01	2,6
NGC288/213	9244	3.15	3.50	...	15.86	0.00	...	1.03	-0.03	2,6
NGC288/229	9866	3.76	5.90	...	16.00	-0.01	...	1.17	-0.04	2
NGC288/230	9450	3.36	8.30	...	15.91	0.02	...	1.08	-0.01	2,6
NGC288/250	9656	3.74	5.10	...	15.96	0.06	...	1.13	0.03	2
NGC288/276	9546	3.25	9.30	...	15.93	0.01	...	1.10	-0.02	2,6
NGC288/291	9621	3.73	10.10	...	15.94	-0.06	...	1.11	-0.09	2
NGC288/292	9126	3.67	10.20	...	15.83	-0.01	...	1.00	-0.04	2
NGC288/305	9441	3.71	9.00	...	15.90	-0.05	...	1.07	-0.08	2
NGC288/306	10058	3.79	1.20	...	16.04	-0.03	...	1.21	-0.06	2
NGC288/318	9634	3.30	7.20	...	15.95	0.01	...	1.12	-0.02	2,6
NGC288/B16	14033	4.15	3.08	0.66	16.57	-0.08	...	1.74	-0.11	5
NGC288/B22	12134	4.01	2.48	0.28	16.49	-0.06	...	1.66	-0.09	5
NGC288/B186	11394	3.94	3.89	0.17	16.42	-0.06	...	1.59	-0.09	5
NGC288/B302	13228	4.15	1.85	0.61	16.58	-0.08	...	1.75	-0.11	5
NGC2808/2333	9057	3.66	5.00	16.80;0.17 ^e	4
NGC2808/2445	7447	3.43	5.00	16.85;0.29 ^e	4
NGC2808/2909	9226	3.68	10.00	16.90;0.15 ^e	4
NGC2808/3159	12050	4.00	5.00	16.97;-0.16 ^e	4
NGC2808/3435	10186	3.80	11.00	16.99;0.03 ^e	4
NGC2808/3715	11194	3.91	4.00	17.00;-0.08 ^e	4
NGC2808/3721	10375	3.82	6.00	17.09;0.00 ^e	4
NGC2808/3841	10046	3.79	13.00	17.04;0.04 ^e	4
NGC2808/3949	9840	3.76	8.00	17.08;0.07 ^e	4
NGC2808/4512	11940	3.99	8.00	17.14;-0.15 ^e	4
NGC2808/4991	10940	3.89	5.00	17.29;-0.06 ^e	4
NGC2808/6427	15311	4.28	6.00	17.57;-0.37 ^e	4
NGC2808/7596	28379	5.01	6.00	17.71;-0.79 ^e	4
NGC2808/9432	23067	4.77	6.00	18.22;-0.67 ^e	4
NGC2808/9655	18923	4.53	7.00	18.29;-0.53 ^e	4
NGC2808/11222	20606	4.63	6.00	18.37;-0.59 ^e	4

Continued on Next Page...

TABLE 4 – Continued

Star ID	T_{eff}	$\log(g)$	$v \sin i$	[Fe/H]	V	$(B-V)$	OTHER	M_V	$(B-V)_0$	Reference
	(K)	(cgs)	(km s^{-1})	(dex)	(mag)	(mag)	(mag)	(mag)	(mag)	

REFERENCES:

- (1) Peterson 1985.
- (2) Peterson et al. 1995.
- (3) Cohen 1997.
- (4) Recio-Blanco et al. 2002.
- (5) Behr 2003a.
- (6) Crocker et al. 1988.
- (7) Moehler et al. 1995.
- (8) Fabbian et al. 2005.

¹ (a) (V-I) Johnson system² (b) u,(u-y) Strömgren system³ (c) F555W,(F439W-F555W) Strömgren system⁴ (d) (U-V) Johnson system⁵ (e) U,(U-B) Johnson system